Clim. Past Discuss., 11, 4329–4389, 2015
www.clim-past-discuss.net/11/4329/2015/
doi:10.5194/cpd-11-4329-2015

Climate of the Past Discussions
Open Access

Stable isotope and calcareous nannofossil assemblage records for the Cicogna section: toward a detailed template of late Paleocene and early Eocene global carbon cycle and nannoplankton evolution

C. Agnini[1,2], D. J. A. Spofforth[3], G. R. Dickens[4,5], D. Rio[1], H. Pälike[6], J. Backman[5], G. Muttoni[7,8], and E. Dallanave[9]

[1]Dipartimento di Geoscienze, Università di Padova, Padova, Italy
[2]Istituto di Geoscienze e Georisorse – Padova, CNR, Padova, Italy
[3]Robertson – CGG GeoSpec, Llandudno, UK
[4]Department of Earth Sciences, Rice University, Houston, Texas, USA
[5]Department of Geological Sciences, Stockholm University, Stockholm, Sweden
[6]MARUM, University of Bremen, Bremen, Germany
[7]Dipartimento di Scienze della Terra "Ardito Desio", Università Statale di Milano, Milano, Italy
[8]ALP – Alpine Laboratory of Paleomagnetism, Peveragno (CN), Italy

[9]Ludwig-Maximilians, Universität München, München, Germany

Received: 7 August 2015 – Accepted: 26 August 2015 – Published: 11 September 2015

Correspondence to: C. Agnini (claudia.agnini@unipd.it)

Published by Copernicus Publications on behalf of the European Geosciences Union.

CPD
11, 4329–4389, 2015

Abstract

We present records of stable carbon and oxygen isotopes, $CaCO_3$ content, and changes in calcareous nannofossil assemblages across an 81 m thick section of upper Paleocene-lower Eocene marine sedimentary rocks now exposed along Cicogna Stream in northeast Italy. The studied stratigraphic section represents sediment accumulation in a bathyal hemipelagic setting from approximately 57.5 to 52.2 Ma, a multi-million-year time interval characterized by perturbations in the global carbon cycle and changes in calcareous nannofossil assemblages. The bulk carbonate $\delta^{13}C$ profile for the Cicogna section, once placed on a common time scale, resembles that at several other locations across the world, and includes both a long-term drop in $\delta^{13}C$, and multiple short-term carbon isotope excursions (CIEs). This precise correlation of widely separated $\delta^{13}C$ records in marine sequences results from temporal changes in the carbon composition of the exogenic carbon cycle. However, diagenesis has likely modified the $\delta^{13}C$ record at Cicogna, an interpretation supported by variations in bulk carbonate $\delta^{18}O$, which do not conform to expectations for a primary signal. The record of $CaCO_3$ content reflects a combination of carbonate dilution and dissolution, as also inferred at other sites. Our detailed documentation and statistical analysis of calcareous nannofossil assemblages show major differences before, during and after the Paleocene Eocene Thermal Maximum. Other CIEs in our lower Paleogene section do not exhibit such a distinctive change; instead, these events are sometimes characterized by variations restricted to a limited number of taxa and transient shifts in the relative abundance of primary assemblage components. Both long-lasting and short-lived modifications to calcareous nannofossil assemblages preferentially affected nannoliths or holococcoliths such as *Discoaster, Fasciculithus, Rhomboaster/Tribrachiatus, Spenolithus* and *Zygrhablithus*, which underwent distinct variations in abundance as well as permanent evolutionary changes in terms of appearances and disappearances. By contrast, placoliths such as *Coccolithus* and *Toweius*, which represent the main component of the assemblages, were characterized by a gradual decline in abundance over time. Com-

CPD
11, 4329–4389, 2015

parisons of detailed nannofossil assemblage records at the Cicogna section and at ODP Site 1262 support the idea that variations in relative and absolute abundance, even some minor ones, were globally synchronous. An obvious link is through climate forcing and carbon cycling, although precise linkages to changes in δ^{13}C records and oceanographic change will need additional work.

1 Introduction

A remarkable interval of global warming occurred from the middle Paleocene to the early Eocene, between approximately 59 and 51 million years ago (Ma). This inference comes from a variety of proxy evidences (Huber and Caballero, 2011; Hollis et al., 2012), including the stable oxygen isotope (δ^{18}O) composition of benthic foraminifera (Fig. 1). The precise timing of this temperature rise remains somewhat unconstrained, because absolute ages across the early Eocene remain unsolidified. Throughout this work, we assume that that the Option-1 (WO-1) time scale presented by Westerhold et al. (2008) is correct (Table 1), but acknowledge that it may be offset by ca 400 kyr for the time interval of interest (Vandenberghe et al., 2012). The magnitude and distribution of the temperature change is also debated. Earth's surface temperatures, at least at high latitudes and in the deep sea, seem to have risen by at least 6 °C from ca. 59 to 51 Ma (Zachos et al., 2008; Bijl et al., 2009; Huber and Caballero, 2011; Hollis et al., 2012). Indeed, the latter date marks the crux of the Early Eocene Climatic Optimum (EECO), the warmest sustained time interval of the Cenozoic (Zachos et al., 2008; Cramer et al., 2009; Hollis et al., 2012). Such a temperature rise is not obvious at low latitudes with current data (Pearson et al., 2007; Huber et al., 2011).

Somehow related to this global warming were a series of major perturbations in the global carbon cycle, as clearly indicated by stable carbon isotope (δ^{13}C) records in benthic foraminifera (Fig. 1) and bulk carbonate in numerous marine sediment sequences (Shackleton, 1986; Corfield, 1994; Cramer et al., 2003; Zachos et al., 2008, 2010; Westerhold et al., 2011; Slotnick et al., 2012). An overall increase in δ^{13}C

CPD
11, 4329–4389, 2015

occurred through most of the Paleocene, which climaxed in a Cenozoic high at ca. 57.5 Ma (Westerhold et al., 2011), commonly referred to as the Paleocene carbon isotope maximum (PCIM). From this time, $\delta^{13}C$ generally decreased to ca 52.5 Ma. However, when examined at higher temporal resolution, multiple $\delta^{13}C$ records show several short-term (< 200 kyr) negative carbon isotope excursions (CIEs) (Cramer et al., 2003; Lourens et al., 2005; Nicolo et al., 2007; Agnini et al., 2009; Zachos et al., 2010; Slotnick et al., 2012). Some of these CIEs clearly coincided with rapid warming (above references). The most prominent and most widely documented example of these "hyperthermals" was the Paleocene-Eocene Thermal Maximum (PETM) at ca 55.5 Ma, but other apparently similar events occurred at ca 53.7 Ma (H1 or Eocene Thermal Maximum 2, ETM-2), and at ca 52.5 Ma (K/X, sometimes called ETM-3).

The early Paleogene in general, and the hyperthermals in particular, have attracted considerable geoscience research. On one level, this is because these time intervals represent a range of possible past analogues for understanding the affects of global warming and massive carbon emissions (cf. Keeling and Whorf, 2004; Zachos et al., 2008). On another level, this is because the long-term and short-term temperature and carbon cycle perturbations provide new perspectives for how Earth surface systems operate. The PCIM probably represents a tremendous storage of ^{13}C-depleted carbon somewhere on Earth's shallow surface (Shackleton, 1986; Kurtz et al., 2003; Komar et al., 2013). In turn, the CIEs probably signify rapid and large inputs of ^{13}C-depleted carbon into the ocean and atmosphere (Dickens et al., 1997; Lourens et al., 2005; Zeebe et al., 2009). The middle Paleocene through early Eocene shows us that Earth's climate and carbon reservoirs were extremely dynamic during past times of global warmth. However, the composition and whereabouts of large quantities of transferable ^{13}C-depleted carbon (e.g., seafloor methane, peat, permafrost) remain uncertain (above references). Indeed, it is not clear if and how the long-term and short-term carbon cycle perturbations were related to one another, or to Earth surface temperatures.

CPD
11, 4329–4389, 2015

The above context presents a series of basic questions to the geoscience community. Two of these are the focus of our study: (1) What is the correct template for understanding carbon cycling during the early Paleogene? Major changes in fluxes of ^{13}C-depleted carbon to the ocean or atmosphere should give predictable and coherent signals in the δ^{13}C of carbon-bearing phases across Earth, as well as the distribution of carbonate dissolution on the seafloor. This is not yet established. For example, several recently published δ^{13}C records (Kirtland-Turner et al., 2014; Slotnick et al., 2015; Payros et al., 2015) do not easily correlate with those at other locations (Cramer et al., 2003; Zachos et al., 2010; Slotnick et al., 2012; 2015a), at least with available stratigraphy. (2) How did marine calcifying organisms respond to major early Paleogene perturbations in temperature and carbon cycling, both in terms of evolution and preservation? The prominent changes in temperature and carbon fluxes almost assuredly caused large variations in seawater pH and carbonate ion concentration (CO_3^{2-}) (Dickens et al., 1997; Kump et al., 2009; Zachos et al., 2005; Zeebe et al., 2009; Leon-Rodriguez and Dickens, 2010; Pälike et al., 2012; Hönisch et al., 2012), although the response should depend on location and carbon fluxes involved (Dickens, 2000; Zeebe and Westbroek, 2003; Komar et al., 2013). Such changes might also affect the ability of living organisms to calcify (Kleypas et al., 2006; Iglesias-Rodriguez et al., 2008; Riebesell et al., 2000, 2008; Stillman and Paganini, 2015), which might impact the fossil record (Agnini et al., 2006; Raffi and De Bernardi, 2008; Erba et al., 2010; Hönisch et al., 2012).

In regards to both questions, calcareous nannoplankton are an obvious group of organisms to focus on. This is because they are a main component of open ocean primary production (Rost and Riebesell, 2004), because they are the dominant output of carbonate from the ocean (Milliman, 1993; Ziveri et al., 1999; Hay, 2004), and because they exhibit marked changes in species composition from the middle Paleocene through the early Eocene (Romein, 1979; Aubry, 1998; Bown et al., 2004; Gibbs et al., 2012). While numerous studies have examined calcareous nannofossils across the PETM from different perspectives (e.g., Bralower, 2002; Stoll and Bains, 2003; Gibbs

CPD
11, 4329–4389, 2015

et al., 2006a, b; Agnini et al., 2007a; Mutterlose et al., 2007; Bown and Pearson, 2009; Jiang and Wise, 2009; Self-Trail et al., 2012), the relationship between these organisms and carbon cycle perturbations before and after this short-lived warming episode remain poorly documented (Gibbs et al., 2012). It seems possible that the high rate of calcareous nannofossil taxonomic evolution (appearances and extinctions), as well as distinct changes in calcareous nannofossil abundance patterns may provide excellent stratigraphic control across the early Paleogene (Bukry, 1973; Perch-Nielsen, 1985; Backman, 1986; Agnini et al., 2014). In turn, if the exact relationship between changes in nannofossil assemblages and global carbon cycle perturbations were known, key time intervals could be identified rapidly for more detailed work. Finally, changes in calcareous nannofossils across the early Paleogene may signal the response of an important part of the overall marine biota to changes in climate and carbon cycling.

Very few sections presently have detailed and coupled records of stable isotopes, carbonate content, and calcareous nannofossil abundances across the broad late Paleocene-early Eocene interval. The two notable examples are Ocean Drilling Program (ODP) Site 1262 (southeast Atlantic) (Agnini et al., 2007; Zachos et al., 2010) and Deep Sea Drilling Project (DSDP) Site 577 (northwest Pacific) (Shackleton, 1986; Dickens and Backman, 2013) (Fig. 2). Here we present geochemical records ($\delta^{13}C$, $\delta^{18}O$ and $CaCO_3$ content) and calcareous nannofossil census data from the Cicogna section in northeast Italy (Figs. 2 and 3). These data are compared with similar information from Sites 1262 and 577. We show that the Cicogna section provides an important template for understanding potential relationships between climate, carbon cycling and the biotic evolution of calcareous nannoplankton.

2 The Cicogna section

The Cicogna section crops out along the Cicogna Stream near the village of Tassei in Belluno Province, northeast Italy (Fig. 3). From a regional geological perspective, the sedimentary rocks of this section belong to the Belluno Basin. This basin represents

CPD
11, 4329–4389, 2015

part of a paleogeographic domain that formed when Jurassic rifting created a series of N–S oriented structural highs (platforms) and lows (basins), which persisted through much of the Paleogene (Bernoulli and Jenkyns, 1974; Bernoulli et al., 1979; Winterer and Bosellini, 1981). Importantly, from the Cretaceous to the middle-late Eocene, expanded deep marine sediment successions accumulated within the basins at 30° N latitude (Stefani and Grandesso, 1991; Agnini et al., 2006; Zattin et al., 2006; Agnini et al., 2011).

The section consists of two lithostratigraphic units (Fig. 3). The lower portion is a well-exposed upper Paleocene and lower Eocene unit referred to as Scaglia Rossa *sensu lato* (Figs. 3 and 4) (Giusberti et al., 2007; Dallanave et al., 2009). The marls of this unit are inferred to represent lithified pelagic and hemipelagic sediment that accumulated at middle to lower bathyal paleodepths, likely between 600 and 1000 m below sea-level but not deeper than 1500 m, during the early Paleogene (Giusberti et al., 2007). The upper portion is a thick early to middle Eocene unit called the Belluno Flysch (Figs. 3 and 4). This unit represents a synorogenic deposit on the flanks of the former Trento and Friuli platforms (Grandesso, 1976; Doglioni and Bosellini, 1987).

Once corrected for bed strike and dip (ca. 315° N; ca. 45°) and bends in the stream, the Scaglia Rossa at Cicogna measures 80 m in terms of stratigraphic height (Dallanave et al., 2009). Furthermore, the section of interest can be subdivided into several subunits (Fig. 4). The lower 20 m is comprised of distinctive alternating beds of gray-greenish to purple marls and calcareous marls, the latter defined by carbonate contents higher than 60 % (Fig. 3c). This is overlain by approximately 9 m of pink-red marls with much less lithologic alternation. At 28.7 m, the sedimentary package is broken sharply by an approximately 3 m thick red to brownish-red interval of clayey marls with sporadic grey-green cm-scale spots and lenses (Fig. 3f, g). This has been called the Clay Marl Unit (CMU), and records the core of the prominent negative $\delta^{13}C$ excursion associated with the PETM at outcrop sites within the Belluno Basin (Agnini et al., 2006, 2007a; Giusberti et al., 2007). Above the CMU, from 31.7 to 39.2 m, the section continues with deposition of rhythmic alternations of marls and calcareous marls (Fig. 3g).

CPD
11, 4329–4389, 2015

Above this 8.5 m thick interval, we observe a very localized presence of spatic calcite at ca. 40.5 m. Genarally, marl/calcareous marl couplets become less evident until approximately 54 m, where such couplets reoccur (Fig. 3d). At 75.5 m, a thin calcarenitic bed is encountered, presaging the onset of Belluno Flysch. This turbidite is followed by a temporary return to hemipelagic sedimentation that ends at 80.6 m. Above, sedimentation of Belluno Flysch begins in earnest (Figs. 3b and 4).

The basic stratigraphy of the Scaglia Rossa in the Cicogna section, including both polarity chron boundaries and key calcareous nannofossil biohorizons has been published (Giusberti et al., 2007; Dallanave et al., 2009). The combined biomagnetostratigraphy indicates that the 81 m of interest spans polarity Chron C25r to Chron 23r, and calcareous nannofossil biozones CP6 to CP10 (Okada and Bukry, 1980) or CNP10 to CNE4 (Agnini et al., 2014). Thus, the section represents a 5.3 million year (Myr) long time interval, from 57.5 to 52.2 Ma on the W0–1 time scale. This also implies an average compacted sedimentation rate (SR) of ca 15 m Myr^{-1}. Although the deposition of hemipelagic sediment might suggest relatively constant SRs over time, the PETM and possibly other hyperthermal events in the Belluno Basin were characterized by higher SRs (Giusberti et al., 2007; Agnini et al., 2009; Tipple et al., 2011; Krishnan et al., 2015).

The Scaglia Rossa at Cicogna appears to record fairly continuous sediment accumulation at moderately high deposition rates. This is important because it affords greater time resolution for paleoclimatic study than most deep ocean sites (Fig. 2), and because it provides a different environmental setting. Much of the detailed work and current understanding of stable carbon isotope stratigraphy and calcareous nannofossil variations across the early Paleogene has come from deep-sea drilling sites, although we note the work in Clarence Valley, New Zealand (Fig. 2) (Nicolo et al., 2007; Slotnick et al., 2012, 2015b; Dallanave et al., 2015). For the Cicogna section, currently lacking are detailed stable isotope and $CaCO_3$ records, as well as detailed calcareous nannofossil assemblage information, which we present here.

CPD
11, 4329–4389, 2015

3 Material and methods

3.1 Samples

A total of 492 samples were chiseled from outcrops along the section. Samples were selected so as be as fresh and unaltered as possible. This included chipping off weathered surfaces while in the field. Each sample was calibrated to height (Fig. 4). Samples then were split, with one portion powdered in an agate ball mill, and subsequently freeze-dried.

3.2 Geochemistry

Each powdered samples was analyzed for bulk sediment stable isotope composition at the Stable Isotope Laboratory, University of Southampton, UK. A known mass ($\sim$ 800 µg) was placed into a headspace vial, dried overnight, and flushed with helium. 10 mL of 100 % phosphoric acid was added to each sample and allowed to react. The liberated CO_2 gas was measured using an EUROPA Scientific GEO 20–20 mass spectrometer fitted with a microCAPS for carbonate analysis. Results are reported in standard delta notation relative to Vienna Pee Dee Belemnite (VPDB). An in-house standard of Carrara Marble, calibrated to NBS-19 Limestone, was measured multiple times to evaluate accuracy and precision. The external analytical precision (1σ), based on these replicate analyses, was 0.028 ‰ for $\delta^{13}C$ and 0.057 ‰ for $\delta^{18}O$.

The amount of $CaCO_3$ in each sample was calculated from the beam height response during isotope mass spectrometer measurements (Spofforth et al., 2010). The liberated CO_2 gas, when squeezed up in the bellows, is measured and generates a current, the beam height. The pressure of CO_2 gas is directly proportional to the beam height and therefore the mass of carbonate in the sample. Over 100 samples of pure $CaCO_3$, with masses between 200 and 480 µg, were analyzed to establish a linear relationship between beam height and carbonate content ($CaCO_3 = mx + b$; $R^2 = 0.94$–

CPD
11, 4329–4389, 2015

0.99). Results were validated by analyzing 30 samples on a C-H-N-O elemental analyzer.

3.3 Calcareous nannofossils

The un-powdered sample split was examined for calcareous nannofossils. Raw sediments were processed to prepare standard smear slides (Bown and Young, 1998). These samples were then examined under a Zeiss light microscope at 1250 × magnification. Calcareous nannofossils were determined using taxonomy proposed by Aubry (1984, 1988, 1989, 1990, 1999), Perch-Nielsen (1985) and Bown (2005).

A total of 200 samples were examined having an average time resolution of ca. 25 kyr. A preliminary qualitative estimate of the abundance and preservation state of calcareous nannofossil assemblages was performed for all samples. An initial large batch (185) was analyzed to provide biostratigraphic data. This information was presented previously (Dallanave et al., 2009). We re-checked and/or refined the positions of some biohorizons by examining 15 additional samples, primarily across some of the CIEs, such as B1/B2, PETM, H1 and H2, and K/X (Cramer et al., 2003). The biostratigraphic schemes previously adopted (Dallanave et al., 2009), are those of Martini (1971) and Okada and Bukry (1980). The new zonal scheme of Agnini et al. (2014) is also used here.

Calcareous nannofossil biostratigraphic results are based on semi-quantitative analyses, which consist in counting the number of specimens of selected taxa present in a prefixed area, 1 mm^2 or 3 vertical traverses (modified after Backman and Shackleton,1983). Calcareous nannofossil paleoecological results are instead based on relative abundances of calcareous nannofossil taxa (%), which are calculated based on at least 300 specimens.

Principal component analysis (PCA) was performed on the percentages of 15 subgroups using the statistical software package, PAST ver. 2.17c (Hammer et al., 2001). Such analysis is often used for examining paleontological data (Watkins and Self-Trail, 1992; Thibault and Gardin, 2010; Marino et al., 2012; Bordiga et al., 2015), as

CPD
11, 4329–4389, 2015

it can point out hypothetical variables (components) that explain much of the variance in a multidimensional data set. The first principal component accounts for the most variability in any dataset examined. Each succeeding component has the highest variance possible relative to the preceding components (Hammer et al., 2001). The chosen subgroups were: *Chiasmolithus, Coccolithus, Ellipsolithus, Discoaster, Ericsonia, Fascicuithus, Girgisia, Octolithus, Prinsius, Sphenolithus, Toweius, Rhomboaster/Tribrachiatus, Zyghrablithus,* reworking, and "others".

4 Results

4.1 Carbon isotopes

The bulk rock δ^{13}C record for the Cicogna section can be described, in a general sense, as a long-term decrease of approximately 3 ‰, punctuated by a series of negative CIEs (Fig. 4). The most prominent low in δ^{13}C coincides with the CMU.

Previously established polarity chron boundaries and key calcareous nannofossil biohorizons at the Cicogna section (Dallanave et al., 2009) provide the stratigraphic framework. Once placed onto a common time scale, in this case WO-1 (Westerhold et al., 2008), the δ^{13}C record at Cicogna is fairly similar to those generated using upper Paleocene and lower Eocene marine carbonate at other locations (Cramer et al., 2003; Zachos et al., 2010; Slotnick et al., 2012). This includes, for example, bulk carbonate δ^{13}C records at ODP Site 1262 and DSDP Site 577 (Fig. 5). The relatively high δ^{13}C values near the base of the section document the late stages of the PCIM, which was centered within C25r (Fig. 1). The overall drop in δ^{13}C across the section marks the long-term global decrease in δ^{13}C that lasted through Chron C24n (Fig. 1). The record contains multiple negative shifts in δ^{13}C. There is, however, an intriguing difference: across the Cicogna section, the long-term 3 ‰ shift in bulk carbonate δ^{13}C values is generally offset from that in bulk carbonate δ^{13}C records at Sites 1262 and 577 by approximately −1 ‰.

CPD
11, 4329–4389, 2015

The superimposed CIEs are considered to correspond to CIEs found in $\delta^{13}C$ records from elsewhere, some of which represent known or inferred hyperthermal events (Cramer et al., 2003; Lourens et al., 2005; Nicolo et al., 2007; Zachos et al., 2010; Slotnick et al., 2012). There are three pairs of CIEs below the CMU (Fig. 4), and during the initial upper Paleocene long-term decline in $\delta^{13}C$. These correspond with the B1/B2, C1/C2 and D1/D2 CIEs documented by others (Cramer et al., 2003; Zachos et al., 2010). Notably, at Site 1262, the B1/B2 CIEs occur during the middle of C25n, and the C1/C2 CIEs occur at the start of C24r (Fig. 5). The same is true at Cicogna. Interestingly, at Cicogna, the B2 and C2 CIEs show greater magnitudes than the B1 and C1 CIEs, and these paired excursions are more pronounced than at all other locations examined to date. An additional paired CIE occurs in the uppermost Paleocene (Fig. 4). This may correlate to a fourth set of late Paleocene CIEs documented at Site 1262 (Zachos et al., 2010).

The lower Eocene portion of the $\delta^{13}C$ record at Cicogna (Fig. 4) begins at the CMU, which marks the PETM (Giusberti et al., 2007; Dallanave et al., 2009). As at many locations, the PETM is characterized by a prominent negative CIE. The shift in $\delta^{13}C$ at Cicogna is approximately −2.5 ‰, a decrease that begins abruptly at 28.7 m and returns more gradually to near pre-excursion values by about 33 m. From approximately 33 to 54 m, the $\delta^{13}C$ curve shows a relatively smooth trend. At 54 m, a pair of CIEs begin, with the first having a magnitude of about 1.0 ‰. These are the H1/H2 events (Cramer et al., 2003), which occurred in the upper part of Chron C24r (Lourens et al., 2005; Zachos et al., 2010; Dickens and Backman, 2013; Dallanave et al., 2015). Above the H1/H2 CIEs, and within Chron C24n, are a series of smaller (0.4 to 0.6 ‰) CIEs. Those at approximately 60, 65 and 72 m, are correlated with the I1/I2, J and K/X events, respectively. In summary, the $\delta^{13}C$ record at Cicogna correlates with that at ODP Site 1262 (Zachos et al., 2010) and DSDP Site 577 (Dickens and Backman, 2013) (Fig. 5), as well as at several other locations (Cramer et al., 2003; Slotnick et al., 2012, 2015b). This is important because it enables comparison and discussion between widely separated sedimentary records within a fairly high-resolution temporal framework.

CPD
11, 4329–4389, 2015

4.2 Oxygen isotopes

The $\delta^{18}O$ values range from −1.08 to −3.64 ‰ with a mean value of −1.96 ‰ and a standard deviation (1σ) of 0.50 ‰ (Fig. 4). However, at the broad scale, $\delta^{18}O$ increases up section, with Paleocene samples averaging −2.10 ‰ and Eocene samples averaging −1.89 ‰. This trend is noteworthy because $\delta^{18}O$ values should decrease up section, if the composition of the $CaCO_3$ was principally reflecting rising global temperatures through the early Eocene. The 1σ of $\delta^{18}O$ values also increases up section, being 0.33 ‰ across Paleocene samples and 0.56 ‰ across Eocene samples.

There is little correlation ($r^2 = 0.014$; $r = 0.12$) between $\delta^{18}O$ and $\delta^{13}C$ values across all samples (Fig. 6). However, most "short-term" CIEs do display drops in $\delta^{18}O$ (Fig. 4). An interval of anomalously low $\delta^{18}O$ values is found from 39.9 to 40.9 m, where the spatic calcite were observed.

4.3 Carbonate content

The $CaCO_3$ content varies between 9.4 and 77.7 % across the sample suite, with a mean value of 54.3 % and a 1σ of 8.2 % (Fig. 4). Two important findings emerge from the $CaCO_3$ content record. First, from 39 to 54 m, where we find limited variance in the $\delta^{13}C$ curve, $CaCO_3$ content averages 52.1 % with a 1σ of 4.9 %. Thus, while the average is similar to that calculated for the entire section, the standard deviation is much less. At Site 1262, the corresponding time interval is also characterized by limited variance in $\delta^{13}C$ values and carbonate contents, the latter inferred from the abundance of Fe counts in XRF scans (Zachos et al., 2010). Second, across all samples, the $CaCO_3$ content co-varies somewhat ($r = 0.29$) with $\delta^{13}C$ (Fig. 6). This is because several lows in $CaCO_3$ content coincide with minima in $\delta^{13}C$, as obvious for the B1/B2, PETM and H1/H2 events (Fig. 4).

CPD
11, 4329–4389, 2015

4.4 Calcareous nannofossils

Calcareous nannofossils are generally abundant, diverse, and moderately well preserved. The sole exception is across a 10 cm interval between 28.75 to 28.85 m, which corresponds to the onset of the CIE that marks the PETM. The three samples from this interval are virtually barren of calcareous nannofossils.

Secondary overgrowth of calcite can partially or wholly blur species-specific morphological features. Such diagenetic alteration, however, only marginal influences the relative and absolute abundance of calcareous nannofossil taxa (Toffanin et al., 2013). Calcite dissolution, on the other hand, can significantly affect the relative abundances of various calcareous nannofossils within a volume of sediment. This, is because the removal of more dissolution susceptible taxa, such as *Toweius* and holococcoliths, necessarily increases the abundance of less dissolution susceptible taxa, such as discoasters (Roth and Thierstein (1972); Adelseck et al., 1973; Roth (1983).Bornemann and Mutterlose, 2008; Toffanin et al., 2013. In general, moderate to strong calcite dissolution also decreases the total abundance of calcareous nannofossils within a volume of sediment (Adelseck et al., 1973; Toffanin et al., 2011). In the Cicogna section, calcite overgrowth on discoasters is the prevalent process affecting calcareous nannofossil assemblages (Plate I). Most assemblages display high abundances (> 1000 specimens mm^{-2}) and a high diversity, which include more fragile taxa. It follows that dissolution has not severely altered most assemblages in samples from the Cicogna section. Rather, the calcareous nannofossil record likely records a genuine paleoecological signal.

Nannofossil assemblages from the Cicogna section display several general trends (Figs. 7–9). At the most basic level, there is a decrease in the total number of nannofossils ($N\,mm^{-2}$) with decreasing age. Paleocene samples average approximately $2600\,N\,mm^{-2}$, whereas Eocene samples above the H1/H2 events average approximately $1200\,N\,mm^{-2}$. This decrease in abundance broadly corresponds to a change in calcareous nannofossil composition, as supported through a series of additional obser-

CPD
11, 4329–4389, 2015

vations. For the calcareous nannofossil assemblages in the Cicogna section (Figs. 7–9):

- *Coccolithus* and *Toweius* constitute nearly half of the assemblages considering the entire section. However, these genera show a clear decrease in abundance up section, with a mean value of 60 % in Paleocene samples and 35 % in Eocene samples.
- *Zyghrablithus bijugatus* shows a low mean value of approximately 4 % in the Paleocene, followed by a sharp increase in the basal part of the Eocene, and a mean value of approximately 25 % up section in the Eocene. Hence, the abundance of this taxon expands on behalf of *Coccolithus* and *Toweius*.
- *Sphenolithus* decreases progressively during the Paleocene, suddenly disappears at the onset of the PETM, before returning to and exceeding pre-PETM values in the lower Eocene. Thus, the abundance of sphenoliths also expands on behalf of *Coccolithus* and *Toweius*.
- *Fasciculithus* shows a severe decline in abundance and species diversity at the onset of the PETM (28.70 m), leading up to an extinction at 34.73 m.
- *Octolithus* is rare throughout most of the studied section, but displays high abundances from approximately 14.7 to 27.5 m in the upper Paleocene.
- *Discoaster* does not show any distinct change in abundance except for a single peak at the onset of the PETM.
- Several Cretaceous and early Paleocene species constitute minor components throughout the section, presumably representing the reworking of sediment. Notably, though, the intervals marked by the PETM, H1/H2 and, to a lesser extent, B1/B2 CIEs are characterized by higher abundances of these older components.

CPD
11, 4329–4389, 2015

– Representatives of placolith genera, such as *Prinsius, Ericsonia, Chiasmolithus* and *Girgisia*, also are minor components of most samples. *Prinsius* displays a marked permanent decrease in abundance from a mean value of approximately 6 to 2.5 % across the Paleocene/Eocene boundary. By contrast, *Ericsonia* does not show a prominent difference in abundance between Paleocene and Eocene assemblages, but instead increases in abundance during known and suspected hyperthermal events.

– The Calcareous Nannofossil Excursion Taxa (CNET), which include *Discoaster araneus* and the genus*Rhomboaster* are present during the CIE of the PETM. The evolution of the *Rhomboaster*/*Tribrachiatus* plexus started at the onset of the PETM, when *Rhomboaster* and *T. bramlettei* first appeared, and continued into the lower Eocene with the successive appearances of *T. contortus* and *T. orthostylus* (Raffi et al., 2005; Agnini et al., 2006, 2007b).

Beyond the above variations, evolutionary appearances and extinctions occur during the studied time interval (Figs. 7–9). Most of these species belong to *Discoaster, Sphenolithus* and the *Rhomboaster/Tribrachiatus* lineage, and include*D. multiradiatus, D. diastypus, D. lodoensis, S. radians, S. anarrhopus, T. bramlettei, T. contortus* and *T. orthostylus*. The biohorizons defined using these species are exceptionally useful for biostratigraphy and, interestingly, often occur close to changes in δ^{13}C.

All assemblage data were used for PCA analysis. This indicates that PC1 (60.6 %) and PC2 (15.6 %) together account for 76.2 % of the variance in the dataset. The PCA graph (Fig. 8) shows that samples can be easily subdivided into three subgroups. The first two populations of samples are distinguished because of their different positions along the *x* axis (PC1). The third population can be separated from the other two because of its different position along the *y* axis (PC2).

CPD
11, 4329–4389, 2015

5 Discussion

5.1 Integrated stratigraphy and a carbon isotope template

Polarity chron boundaries and calcareous nannofossil biohorizons (Table 1; Fig. 4) provide a very good stratigraphic framework for the Cicogna section. All these biohorizons, including additional ones defined here, align in same stratigraphic order when compared to other locations, such as ODP Site 1262 and DSDP Site 577 (Table 1; Fig. 11). The Cicogna section represents sediment accumulation between 57.5 and 52.2 Ma on the WO-1 time scale (Dallanave et al., 2009). The average SR was ~ 15.2 m Myr^{-1}, although this must have varied (Figs. 3 and 11). The CMU, which marks the "core" of the PETM and ca. 80–100 kyr, had higher SR than much of the record (Dallanave et al., 2009; Krishnan et al., 2015).

Once placed into the above stratigraphic framework, the bulk carbonate δ^{13}C profile documented at Cicogna nicely correlates to that generated at ODP Site 1262 (Fig. 5). In fact, it is similar to δ^{13}C profiles generated at multiple locations (Fig. 2), as long as records have been properly calibrated in both depth and time domains. This includes accounting for core stretching and core gaps at scientific drilling sites, such as at DSDP Site 577 (Dickens and Backman, 2013), and accounting for changing strike and dip along land sections, such as done at Cicogna (Fig. 3). During late Paleocene and early Eocene times, the Cicogna section records the long-term decrease in δ^{13}C. Superimposed on this drop were multiple, often paired, negative CIEs. The PETM definitively represents the most prominent CIE, but several other CIEs occurred before and after. Importantly, the relative positions of polarity chron boundaries, key calcareous nannofossil biohorizons and CIEs at Cicogna align with those found at other locations (Table 1; Figs. 5 and 11).

A very recognizable δ^{13}C pattern spans the late Paleocene through the early Eocene at several locations (Cramer et al., 2003; Nicolo et al., 2007; Galeotti et al., 2010; Zachos et al., 2010; Slotnick et al., 2012, 2015b), although the total number of CIEs remains uncertain. At Cicogna, the problem lies in the interval surrounding the K/X

CPD
11, 4329–4389, 2015

event, which broadly corresponds to the start of the EECO (see discussion in Slotnick et al., 2012). We cannot confirm with our sample resolution whether a series of short-term, small amplitude CIEs mark this time, an idea suggested from $\delta^{13}C$ records of the Clarence Valley sections (Slotnick et al., 2012, 2015b). However, as at other locations, such as Site 1262, no significant CIEs occurred within the 1.6 Myrs following the PETM and before the H-1/ETM-2 event (Fig. 5).

The time-correlative $\delta^{13}C$ template found in multiple, widespread marine sequences must reflect changes in the $\delta^{13}C$ composition of the ocean. In turn, the compositional change must represent variations in fluxes of highly ^{13}C-depleted carbon to and from the ocean or atmosphere, such as changes in the release and storage of organic carbon (Shackleton, 1986; Dickens et al., 1997; Kurtz et al., 2003; Deconto et al., 2010; Komar et al., 2013). The $\delta^{13}C$ record at Cicogna offers no direct insight on the location of this carbon (e.g., seafloor methane, permafrost, peat). However, it does support an important concept: the magnitudes of given CIEs appear somewhat related to one another and to the long-term $\delta^{13}C$ record. In particular, the PETM occurred about halfway between the long-term high and low in $\delta^{13}C$, and heralded a relatively long time interval with no negative CIEs. A generic explanation is that a very large mass of ^{13}C-depleted carbon was injected from some organic reservoir into the ocean or atmosphere during the PETM, and that the reservoir needed to recharge for considerable time before another such injection (H-1/ETM-2) could occur (Dickens et al., 2003; Kurtz et al., 2003; Lunt et al., 2011; Komar et al., 2013).

The overall −1 ‰ offset of the $\delta^{13}C$ curve between the records at Cicogna and at Sites 577 and 1262 (Fig. 5) warrants brief discussion. It probably does not reflect wholesale diagenesis and resetting of the primary signal at any of these sections. Otherwise, a recognizable correlative $\delta^{13}C$ record and well-preserved nannofossils (Plate I) would not be found at all three locations. In fact, it is difficult to modify the original $\delta^{13}C$ composition of carbonate over appreciable distance (> than several meters) in marine sedimentary sequences dominated by fine grained calcite, even those now exposed on land as lithified rock, such as at Cicogna or in the Clarence Valley. This is

CPD
11, 4329–4389, 2015

because the carbon water/rock ratio would always remain low, because almost all carbon would always exist in carbonate, and because temperature minimally influences carbon isotope fractionation (Matter et al., 1977; Scholle and Arthur, 1980; Frank et al., 1999). Instead, the offset in the $\delta^{13}C$ curves probably relates to differences in the composition of original carbonate, a concept that we return to later.

However, local dissolution and re-precipitation of carbonate definitely has occurred in the Cicogna section. This can be observed by the overgrowths on discoasters and *Rhomboaster/Tribrachiatus* (Plate I). This process should dampen the original CIEs, because on the meter-scale, dissolution and re-precipitation of carbonate would involve $\delta^{13}C$ gradients in the dissolved inorganic carbon (DIC) of surrounding pore water (Matter et al., 1977; Scholle and Arthur, 1980). This may explain, in part, why the magnitude of CIEs in bulk carbonate records are often muted relative to those found in other carbon-bearing phases (Slotnick et al., 2015b).

5.2 Oxygen isotopes and a problem recording past temperatures

The $\delta^{18}O$ record at Cicogna is intriguing because many of the CIEs are characterized by negative excursions, but the absolute values of $\delta^{18}O$ generally and unexpectedly increase up section (Fig. 4). Similar results have been documented in bulk carbonate stable isotope records at other locations, such as ODP Site 1215 (Leon-Rodriguez and Dickens, 2010) and Mead Stream (Slotnick et al., 2012). Even the $\delta^{18}O$ record of bulk carbonate at Site 1262 shows minimal long-term change from the late Paleocene to the early Eocene (Zachos et al., 2010), the time when high-latitude surface temperatures and deep ocean temperatures presumably increased by 5–6 °C, and one might expect a > 1 ‰ decrease in the $\delta^{18}O$ of marine carbonate.

Like previous workers, we cannot discount the notion that temperatures at low and high latitudes responded differently across the early Paleogene (Pearson et al., 2007; Huber and Caballero, 2011). Unlike for carbon isotopes, however, local dissolution and re-precipitation of carbonate should significantly impact the $\delta^{18}O$ of marine carbonate. This is because the oxygen water/rock ratio would be high before lithification, and be-

CPD
11, 4329–4389, 2015

cause temperature strongly influences oxygen isotope fractionation (Matter et al., 1977; Scholle and Arthur, 1980; Frank et al., 1999). In general, as calcite-rich sediments and surrounding pore water become buried to higher temperatures along a geothermal gradient, local dissolution and re-precipitation of carbonate should shift carbonate $\delta^{18}O$ to lower values (above references; Schrag et al., 1995). It is likely that, during sediment burial, the bulk carbonate $\delta^{18}O$ records in many lower Paleogene sections, including at Cicogna, have been modified. We suggest that a signal of surface ocean temperature changes remains in the Cicogna section, which gives rise to short-term $\delta^{18}O$ excursions that coincide with CIEs and several known or suspected hyperthermal events. However, the entire $\delta^{18}O$ record at this location likely has shifted to more negative values preferentially with increasing burial depth and age. This partly explains the observed relationship between bulk carbonate $\delta^{13}C$ and $\delta^{18}O$, which lies along a trajectory expected for diagenesis (Fig. 6). A potential test of this idea would be to show that the overgrowths on nannofossils (Plate I) have a significantly lower $\delta^{18}O$ than the primary core carbonate of nannofossil tests.

5.3 Calcareous nannofossil assemblages within the context of correlative stable isotope records

A detailed stable carbon isotope curve provides a powerful means to place past changes in calcareous nannofossil assemblages into a highly resolved framework. This is because, as implied above, truly global changes in the $\delta^{13}C$ composition of the ocean should occur within the cycling time of carbon through ocean, which is < 2000 years at present-day and presumably for the entire Cenozoic (Shackleton, 1990; Dickens et al., 1997).

Across the study interval at Cicogna, several calcareous nannofossil taxa appear or disappear (Table 1). Moreover, their abundances also change between these horizons (Figs. 7–9). One might hypothesize that these changes in nannofossil assemblages were related to the established (e.g., the PETM, H1/ETM-2 and K/X) and potential (e.g., the B1/B2, I1/I2) hyperthermal events that occurred during the late Paleocene

CPD
11, 4329–4389, 2015

and early Eocene (Figs. 1 and 5). However, the timing between recorded evolutionary appearances and extinctions of calcareous nannofossils and perturbations in $\delta^{13}C$ are variable (Figs. 7–9). For instance, several significant calcareous nannofossil changes observed close to H1/H2 hyperthermals (e.g., B *T. othostylus*, B *S. radians*, B *S. villae*, Tc *D. multiradiatus,* T *T. contortus*) predate these events. By contrast, several biotic changes observed close to the B1/B2 CIEs (e.g., B *D. delicatus,* Tc *S. anarrhopus,* B *D. multiradiatus*, T *Ericsonia robusta*) happened at the end of these events. The PETM provides the only case when a negative CIE event precisely corresponds to major changes in calcareous nannofossil assemblages.

Profound changes in calcareous nannofossil assemblages occurred across the PETM in several locations (Fig. 2), both in terms of relative abundances and increases in origination and extinction rates (Aubry, 1998; Bown et al., 2004; Raffi et al., 2005; Agnini et al., 2007a; Gibbs et al., 2006a; Self-Trail et al., 2012). At Cicogna, the assemblages show remarkable, though mostly transient, relative abundance variations across the PETM, including an increase in *Coccolithus*, a decrease in *Zygrhablithus, Sphenolithus, Toweius* and *Prinsius*, and an extinction of most fasciculith species (Fig. 8). Not surprisingly, these changes are very similar to those in the Forada section, which is also located in the Belluno Basin (Agnini et al., 2007a).

Although these changes in the relative abundance of taxa alone represent a notable differentiation with respect to background conditions, most of the changes are transient and/or local when compared with other datasets (Bralower, 2002; Gibbs et al., 2006b; Agnini et al., 2007b; Angori et al., 2007; Mutterlose et al., 2007). For instance, an increase in abundance of *Discoaster* and *Fasciculithus* was reported for some of the PETM section studied (e.g., Bralower, 2002; Bralower and Tremolada, 2004; Raffi et al., 2009), but these assemblage variations were not observed in other sections (e.g., Gibbs et al., 2006; Agnini et al., 2007a; Self-Trail et al., 2012). The only global calcareous nannofossil assemblage features of the PETM are represented by the evolutionary appearance of *Rhomboaster/Tribrachiatus* lineage, the presence during the

CPD
11, 4329–4389, 2015

CIE of short-lived species such as *Discoaster areneus*, and the disappearance of several species of fasciculiths (Raffi et al., 2005; Agnini et al., 2007a).

While changes in calcareous nannoplankton assemblages during the PETM have been investigated at high resolution at different locations (e.g., Bralower, 2002; Gibbs et al., 2006; Agnini et al., 2007a), the longer-term perspective in which such changes occurred during the early Paleogene has remained uncertain (Gibbs et al., 2012). The record at Cicogna provides this opportunity.

The PCA analysis of calcareous nannofossil census data (%) indicates that two principal components (PC1 and PC2) account for most (76.2 %) of the variability in our 15 subgroups. This permits the study samples to be subdivided into three subgroups (Fig. 11). The first two populations of samples are distinguished because of a major difference along an *x* axis representing PC1, whereas the third population stands out because of a significant difference along a *y* axis representing PC2. Importantly, each of these three populations constitutes a homogeneous group in the time domain: Group 1 includes all the upper Paleocene samples (Paleocene samples and B1/B2 events); Group 2 consists of almost all the lower Eocene samples (Eocene samples, H1/H2 events and K event); Group 3 comprises samples that span the PETM (PETM core and PETM recovery), and two samples that come from sediment deposited during the core of H1 and B2 events (Fig. 11). These results indicate that late Paleocene calcareous nannofossil assemblages are statistically different in their composition from those of early Eocene samples. Moreover, the calcareous nannofossil assemblages across the PETM, and the climax of the B2 and H1 events, are statistically different from those of either the late Paleocene or the early Eocene.

The general shift in the relative abundance of placoliths (i.e., *Coccolithus, Toweius* and *Prinsius*), the major component of the late Paleocene assemblages, to nannoliths/holococcoliths (i.e., *Sphenolithus* and *Zygrhablithus*), the major component of the early Eocene assemblages, largely explains the PC1 component. Differently, the PC2 values are quite similar for Paleocene and Eocene samples, except for those of the PETM. This suggests that PC2 account for variations in calcareous nannofossil as-

CPD
11, 4329–4389, 2015

semblages likely related to the peculiar paleoenviromental conditions occurred during the PETM. One can hypothesize that altered chemical parameters of sea surface waters (higher temperatures, oligotrophy/eutrophy, carbonate saturation state, etc.) could have driven the observed changes in calcareous nannoplankton communities.

Statistical analysis of our data at Cicogna does not highlight any prominent short-term changes in calcareous nannofossil assemblages, other than across the PETM and perhaps the B2 and H1 events. However, several biohorizons occur around the B1/B2 events. Specifically, these are the Bc *Z. bijugatus*, the transitory high abundance of *Octolithus* spp., the evolutionary onset of the *D. delicatus/D. multiradiatus* lineage, the presence of the short-ranged *E. robusta*, the final radiation of late Paleocene fasciculiths (i.e., *F. richardii* group, *F. hayi, F. lilianae, F. alanii*), and the Tc of *S. anarrhopus*. All these happened at Cicogna and at Site 1262 within Chron C25n (Agnini et al., 2007b; Dallanave et al., 2009; Fig. 11), which spanned only 0.54 Myr (Westerhold et al., 2008). These quasi-synchronous events are intriguing because while the various nannofossils represent only minor components of late Paleogene assemblages, they were destined to become either an abundant constituent of Eocene populations (e.g., *Z. bijugatus* and the *D. delicatus/D. multiradiatus* lineage), or extinct after having been a distinctive element of Paleocene assemblages (e.g. *Fasciculithus* spp. and *S. anarrhopus)*. Following the PCIM, the long-term increase in temperature and decrease in and δ^{13}C (Fig. 1) coincided with a series of minor changes in nannofossil assemblages, which subsequently became important, presumably for evolutionary reasons.

Similar to the late Paleocene, calcareous nannofossil assemblages after the PETM do not show major rearrangements of common taxa during the early Eocene. Instead, minor components of these assemblages exhibit a sequence of closely spaced biohorizons. The sequence of these biohorizons is: T *Fasciculithus,* B *D. diastypus*, B *T.contortus,* T *T. bramlettei*, Tc *D. multiradiatus,* T *T. contortus*, B *T. orthostylus,* B *S. radians,* T *D.multiradiatus,* B *D. lodoensis,* B *G. gammation* and Bc *D. lodoensis* (Table 1). Within the resolution of available paleomagnetic and δ^{13}C data, all these biohorizons are virtually synchronous between the Cicogna section and ODP Site 1262 (Fig. 11).

CPD
11, 4329–4389, 2015

They also almost all happened at the same time at Site 577 (Dickens and Backman, 2013), although the precise correlation remains uncertain, given problems with coring disturbance and subtleties in age models at this location. Importantly, for stratigraphic purposes, the B and Bc of *D. lodoensis* are approximately coeval at all three locations and spaced apart by about 750 kyr. Unless one examines samples in detail, these two biohorizons can be confused and result in an erroneous assignment of early Eocene ages.

The evolutionary appearances and extinctions amongst early Eocene nannofossil assemblages may suggest the presence of unsteady communities living in an extreme climate in which alterations of environmental conditions, even minor, might trigger evolutionary changes or prominent variations in abundances of a limited number of taxa that typically do not represent the dominant component of assemblages. This could be explained by the general higher tolerance of cosmopolitan taxa to variations in environmental conditions (Boucot, 1975; Winter et al., 1994). In contrast, highly specialized taxa, ones adapted to a particular ecological niche, may display greater sensitivity to modifications in the photic zone environment (MacArthur and Wilson, 1967; Pianka, 1970; Baumann et al., 2005).

In summary, several genera of calcareous nannofossils, such as *Rhomboaster, Tribrachiatus, Sphenolithus, Discoaster* and *Zygrhablithus* were, at least to some extent, affected during the late Paleocene-early Eocene transition, because they show an increased rate of taxonomic evolution (Fig. 11). These are all minor groups in terms of overall abundance in most lower Paleogene sediment sequences, and they all belong to nannoliths and holococcoliths. It appears that these organisms were more sensitive to environmental changes than heterococcoliths, for example the cosmopolitan genera *Coccolithus* and *Toweius*.

5.4 Early Paleogene calcareous nannofossil evolution

Any comprehensive paleoenvironmental interpretation involving early Paleogene calcareous nannofossils remains tentative because many taxa, such as *Rhom-*

CPD
11, 4329–4389, 2015

boaster/Tribrachiatus, *Discoaster, Sphenolithus* and *Zygrhablithus*, are extinct. Still, some single species or species groups are considered to be useful for reconstructions of paleoenvironmental conditions (Geisen et al., 2004). From that viewpoint, we provide here a scenario in which late Paleocene-early Eocene calcareous nannofossil evolution is interpreted based on holococcoliths/nannoliths ecology and classical biogeographic models.

Modern holococcoliths consist of numerous tiny rhombohedral calcite crystallites considered as haploid stages of certain heterococcolithophores, which can live in just about any marine photic zone environment, although higher abundances and diversity are typical in oligotrophic settings (Billard and Inouye, 2004). The most common Paleogene holococcolith was *Zygrhablithus bijugatus.* This taxon has been interpreted as a *K* selected species more adapted to stable environments and oligotrophic conditions (Aubry, 1998; Bralower, 2002; Tremolada and Bralower, 2004; Agnini et al., 2007; Self-Trail et al., 2012). Nannolith is a term used to describe peculiar morphtypes usually observed in association with coccoliths, but lacking the typical features of hetero- or holococcoliths. *Ceratolithus cristatus,* a modern nannolith, has been observed on the same cell together with *Neosphaera coccolithomorpha* (Alcolber and Jordan, 1997), suggesting that the nannolith stage (*C. cristatus*) corresponds to the holococcolith stage in other taxa (Young et al., 2005). Paleogene nannoliths include taxa with peculiar morphologies such as *Discoaster, Fasciculithus* and *Sphenolithus*. These genera have often been associated with warm waters and oligotrophic environments and are almost unanimously interpreted as *K* selected taxa (Haq and Lohmann, 1976; Backman, 1986; Wei and Wise, 1990; Bralower, 2002; Gibbs et al., 2004, 2006a, b; Agnini et al., 2007a). *K* strategists fluctuate at or near the carrying capacity (*K*) of the environment in which they thrive (MacArthur and Wilson, 1967) and they are usually characterized by long individual life-cycles and low reproductive potential. The *K* selected strategy is advantageous in highly stable, typically oligotrophic environments, which allow the evolution of stenotopy and where organisms compete by specialization and partition-

CPD
11, 4329–4389, 2015

ing (Premoli Silva and Sliter, 1999). The narrow range of adaptability to changes of habitats or ecological conditions stimulates an increasingly rapid speciation.

At present, it is commonly accepted that modern holococcolithophores and nannoliths are not autonomous but stages in the life cycle of heterococcolith-covered oceanic species, the passage between the two stages may be triggered by environmental factors (Billard and Inouye, 2004).

Hence, though Paleogene holococcoliths/nannoliths have no direct descendants in present-day oceans, modern taxa likely share similar physiological features with Paleogene species. If this is the case, the increase in relative abundance of holococcoliths and nannoliths at the expense of heterococcoliths as well as the higher rates of evolution shown by holococcoliths and nannoliths may suggest relatively stable, though extreme, conditions in which highly specialized taxa belonging holococcolith/nannolith group could flourish and rapidly evolve. This scenario is consistent with the idea, based on laboratory and modern ocean data, that the calcareous nannoplankton response to environmental/climatic changes is species or group specific rather than homogeneous across the entire assemblage (Riebesell et al., 2000; Langer et al., 2006; Iglesias-Rodriguez et al., 2008; Lohbeck et al., 2012). Variations in the thermal and chemical structure of photic zone waters may thus account for the observed changes in the early Paleogene calcareous nannofossil assemblages.

5.5 Carbon isotope of surface waters during the early Paleogene

Like Cicogna, well-preserved calcareous nannofossils dominate bulk sediment carbonate contents of early Paleogene strata at Sites 577 and 1262 (Backman, 1986; Zachos et al., 2004; Dickens and Backman, 2013). Given that the nannofossil assemblages are fairly similar (Fig. 11), a really basic question returns: why is the overall early Paleogene bulk carbonate $\delta^{13}C$ record at Cicogna less by approximately 1 ‰? A cursory examination of early Paleogene bulk carbonate $\delta^{13}C$ records from other sites of the North Atlantic/western Tethys region (e.g., Sites 550 and 1051; Fig. 2) shows a commonality: these locations also display negative 0.5 to 1 ‰ offsets relative to correlative

CPD
11, 4329–4389, 2015

records at Sites 577 and 1262 (Cramer et al., 2003). The $\delta^{13}C$ of DIC in modern ocean surface waters (< 100 m) ranges by almost 2‰, with generally lower values across broad regions of greater upwelling (Kroopnick, 1985; Tagliabue and Bopp, 2008). It is possible that bulk carbonate $\delta^{13}C$ values in early Paleogene North Atlantic sections record lower values than locations near the Equator or in southern latitudes because of different past ocean circulation.

6 Conclusions

We generate records of bulk carbonate $\delta^{13}C$ and $\delta^{18}O$, $CaCO_3$ content and calcareous nannofossil assemblages from the Cicogna section, a marine sedimentary succession that now crops out along a stream in the Southern Alps of northeast Italy. The combined geochemical and calcareous nannofossil results allow us to generate a detailed stratigraphy for the section, as well as to explore relationships between stable isotope variations and nannofossil assemblages. Most lower Paleogene sections examined to date lack such coupled data sets.

The $\delta^{13}C$ record and calcareous nannofossil assemblages show that the section spans ~ 5.3 Myr of the late Paleocene and early Eocene interval, from 57.5 to 52.2 Ma on the WO-1 timescale. This is consistent with previous paleomagnetic information and preliminary calcareous nannofossil biostratigraphy (Dallanave et al., 2009), but provides a more detailed stratigraphic framework, one appropriate for correlations to other locations around the world. In particular, the fairly well resolved $\delta^{13}C$ record shows long-term and short variations that correspond to those found in several other sections, including an established series of negative CIEs. The most prominent CIE marks the PETM, while other less pronounced CIEs represent the H-1, K/X and other "events" documented elsewhere. The $\delta^{13}C$ variations observed at Cicogna clearly reflect global changes in the fluxes of carbon to and from the ocean and atmosphere.

PCA analysis shows that the PETM, the most intense among the late Paleocene–early Eocene hyperthermals, represents a unique calcareous nannofossil assemblage

CPD
11, 4329–4389, 2015

composition. Late Paleocene and early Eocene assemblages are distinctly different according to the PCA analysis, which thus shows three distinct sample clusters based on taxonomy. This suggests that the brief PETM episode of extreme warming was able to permanently modify the make-up of the assemblages thanks to an increase in the rate of taxonomic evolution (Gibbs et al., 2006a). Less prominent hyperthermal events do not show significant variations in the main components of the assemblages but rather are characterized by a series of changes affecting a limited number of rare taxa, likely less tolerant to alterations of the environment of their habitats.

More common taxa, essentially consisting of placoliths, such as the cosmopolitan *Coccolithus* and *Toweius*, display a progressive long-term decrease interrupted by transient changes in their relative abundance but virtually no extinction or origination events occur in these groups during the pertinent time interval. Species belonging to nannoliths and holococcoliths (*Discoaster, Fasciculithus, Rhomboaster/Tribrachiatus, Spenolithus* and *Zygrhablithus*), generally show a higher rate of evolution and a higher concentration of biohorizons close to $\delta^{13}C$ perturbations. In conclusion, calcareous nannoplankton show a different response of the various components of the assemblages, this is consistent with a species or taxonomic unit sensitivity of calcareous phytoplankton to paleoenviromental perturbations. This evolutionary climate-forced model is supported by data from ODP Site 1262, which demonstrate that these changes are global and synchronous between middle latitudes in the Western Tethys region and the South Atlantic.

The Supplement related to this article is available online at doi:10.5194/cpd-11-4329-2015-supplement.

Acknowledgements. C. Agnini would like to thank Carlotta Betto for preparing smear slides for calcareous nannofossil analyses. We also acknowledge valuable comments from the referees, XX and YY. Funding for this work came from several sources. Primary support came from a MIUR grant to C. Agnini, E. Dallanave and D. Rio (PRIN 2010–2011 – prot. 2010X3PP8J_003.

CPD
11, 4329–4389, 2015

J. Backman acknowledges support from the Swedish Research Council. G. R. Dickens received funding from a National Science Foundation (NSF) grant (NSF-FESD-OCE-1 338 842).

References

Adelseck Jr., C. G., Geehan, G. W., and Roth, P. H.: Experimental evidence for the selective dissolution and overgrowth of calcareous nannofossils during diagenesis, Geol. Soc. Am. Bull., 84, 2755–2762, 1973.

Agnini, C., Muttoni, G., Kent, D. V., and Rio, D.: Eocene biostratigraphy and magnetic stratigraphy from Possagno, Italy: the calcareous nannofossil response to climate variability, Earth Planet. Sc. Lett., 241, 815–830, doi:10.1016/j.epsl.2005.11.005, 2006.

Agnini, C., Fornaciari, E., Rio, D., Tateo, F., Backman, J., and Giusberti, L.: Responses of calcareous nannofossil assemblages, mineralogy and geochemistry to the environmental perturbations across the Paleocene/Eocene boundary in the Venetian Pre–Alp, Mar. Micropaleontol., 63, 19–38, doi:10.1016/j.marmicro.2006.10.002, 2007a.

Agnini, C., Fornaciari, E., Raffi, I., Rio, D., Röhl, U., and Westerhold, T.: High-resolution nannofossil biochronology of middle Paleocene to early Eocene at ODP Site 1262: implications for calcareous nannoplankton evolution, Mar. Micropaleontol., 64, 215–248, doi:10.1016/j.marmicro.2007.05.003, 2007b.

Agnini, C., Macrì, P., Backman, J., Brinkhuis, H., Fornaciari, E., Giusberti, L., Luciani, V., Rio, D., Sluijs, A., and Speranza, F.: An Early Eocene carbon cycle perturbation at 52.5 Ma in the Southern Alps: chronology and biotic response, Paleoceanography, 24, PA2209, doi:10.1029/2008PA001649, 2009.

Agnini, C., Fornaciari, E., Giusberti, L., Grandesso, P., Lanci, L., Luciani, V., Muttoni, G., Pälike, H., Rio, D., Spofforth, D. J. A., and Stefani, C.: Integrated bio-magnetostratigraphy of the Alano section (NE Italy): a proposal for defining the middle-late Eocene boundary, Geol. Soc. Am. Bull., 123, 841–872, doi:10.1130/B30158.1, 2011.

Agnini, C., Fornaciari, E., Raffi, I., Catanzariti, R., Pälike, H., Backman, J., and Rio, D.: Biozonation and biochronology of Paleogene calcareous nannofossils from low and middle latitudes, Newslett. Stratigr., 47, 131–181, doi:10.1127/0078-0421/2014/0042, 2014.

Alcober, J. A. and Jordan, R. W.: An interesting association between *Neosphaera coccolithomorpha* and *Ceratolithus cristatus*, Eur. J. Phycol., 32, 91–93, 1997.

CPD
11, 4329–4389, 2015

Angori, E., Bernaola, G., and Monechi, S.: Calcareous nannofossil assemblages and their response to the Paleocene-Eocene Thermal Maximum event at different latitudes: ODP Site 690 and Tethyan sections, Geol. Soc. Am. Spec. Pap., 424, 69–85, doi:10.1130/2007.2424(04), 2007.

Aubry, M.-P.: Handbook of Cenozoic Calcareous Nannoplankton, book 1, Ortholithae (Discoaster), Am. Mus. Nat. Hist. Micropaleontol. Press, New York, 1–263, 1984.

Aubry, M.-P.: Handbook of Cenozoic Calcareous Nannoplankton, book 2, Ortholithae (Holococcoliths, Ceratoliths, Ortholiths and Other), Am. Mus. Nat. Hist. Micropaleontol. Press, New York, 1–279, 1988.

Aubry, M.-P.: Handbook of Cenozoic Calcareous Nannoplankton, book 3, Ortholithae (Pentaliths and Other), Heliolithae (Fasciculiths, Sphenoliths and Others), Am. Mus. Nat. Hist. Micropaleontol. Press, New York, 1–279, 1989.

Aubry, M.-P.: Handbook of Cenozoic Calcareous Nannoplankton, book 4, Heliolithae (Helicoliths, Cribriliths, Lopadoliths and Other), Am. Mus. Nat. Hist. Micropaleontol. Press, New York, 1–381, 1990.

Aubry, M.-P.: Early Paleogene calcareous nannoplankton evolution: a tale of climatic amelioration, in: Late Paleocene–early Eocene Biotic and Climatic Events in the Marine and Terrestrial Records, Columbia University Press, New York, 158–201, 1998.

Aubry, M.-P.: Handbook of Cenozoic Calcareous Nannoplankton, book 5, Heliolithae (Zygoliths and Rhabdoliths), Am. Mus. Nat. Hist. Micropaleontol. Press, New York, 1–368, 1999.

Aubry, M.-P.: Late Paleocene–early Eocene sedimentary history in western Cuba: implications for the LPTM and for regional tectonic history, Micropaleontol., 45, 5–18, 1999.

Backman, J.: Late Paleocene to middle Eocene calcareous nannofossil biochronology from the Shatsky Rise, Walvis Ridge and Italy, Palaeogeogr. Palaeocl., 57, 43–59, 1986.

Backman, J. and Shackleton, N. J.: Quantitative biochronology of Pliocene and early Pleistocene calcareous nannoplankton from the Atlantic, Indian and Pacific Oceans, Mar. Micropaleontol., 8, 141–170, doi:10.1016/0377-8398(83)90009-9, 1983.

Banner, J. L. and Hanson, G. N.: Calculation of simultaneous isotopic and trace element variations during water rock interaction with applications to carbonate diagenesis, Geochim. Cosmochim. Ac., 54, 3123–2137, doi:.org/10.1016/0016-7037(90)90128-8, 1990.

Baumann, K.-H., Andruleit, H., Böckel, B., Geisen, M., and Kinkel, H.: The significance of extant coccolithophores as indicators of ocean water masses, surface water temperature, and palaeoproductivity: a review, Palaeontol. Z., 79, 93–112, 2005.

CPD
11, 4329–4389, 2015

Bernoulli, D. and Jenkyns, H. C.: Alpine, Mediterranean, and Central Atlantic Mesozoic facies in relation to the early evolution of the Tethys, in: Modern and Ancient Geosynclinal Sedimentation, edited by: Dott Jr., R. H. and Shaver, R. H., Society for Sedimentary Geolology (SEPM) Special Publication, 19, 19–160, 1974.

Bernoulli, D., Caron, C., Homewood, P., Kalin, O., and Van Stuijvenberg, J.: Evolution of continental margins in the Alps: Schweiz, Miner. Petrol., 59, 165–170, 1979.

Bijl, P. K., Schouten, S., Sluijs, A., Reichart, G. J., Zachos, J. C., and Brinkhuis, H.: Early Palaeogene temperature evolution of the southwest Pacific Ocean, Nature, 461, 776–779, doi:10.1038/nature08399, 2009.

Billard, C. and Innouye, I.: What is new in coccolithophore biology?, in: Coccolithophores – From Molecular Processes to Global Impact, Springer, Berlin, 1–29, 2004.

Bordiga, M., Henderiks, J., Tori, F., Monechi, S., Fenero, R., and Thomas, E.: The Eocene–Oligocene transition at ODP Site 1263, Atlantic Ocean: decreases in nannoplankton size and abundance and correlation with benthic foraminiferal assemblages, Clim. Past Discuss., 11, 1615–1664, doi:10.5194/cpd-11-1615-2015, 2015.

Bornemann, A. and Mutterlose, J.: Calcareous nannofossil and $\delta^{13}C$ records from the Early Cretaceous of the Western Atlantic Ocean: evidence for enhanced fertilization across the Berriasian–Valanginian transition, Palaios, 23, 821–832, 2008.

Boucot, A. J.: Evolution and Extinction Rate Controls, Elsevier, Amsterdam, the Netherlands, 250 pp., 1975.

Bown, P. R.: Paleogene calcareous nannofossils from the Kilwa and Lindi areas of coastal Tanzania: Tanzania Drilling Project Sites 1 to 10, J. Nannoplankt. Res., 27, 21–95, 2005.

Bown, P. and Pearson, P.: Calcareous plankton evolution and the Paleocene/Eocene thermal maximum event: new evidence from Tanzania, Mar. Micropaleontol., 71, 60–70, doi:10.1016/j.marmicro.2009.01.005, 2009.

Bown, P. R. and Young, J. R.: Techniques, in: Calcareous Nannofossil Biostratigraphy, Chapman & Hall, London, 16–28, 1998.

Bown, P. R., Lees, J. A., and Young, J. R.: Calcareous nannoplankton evolution and diversity through time, in: Coccolithophores – From Molecular Processes to Global Impact, Springer, Berlin, 481–508, 2004.

Bralower, T. J.: Evidence of surface water oligotrophy during the Paleocene–Eocene thermal maximum: nannofossil assemblage data from Ocean Drilling Program Site 690, Maud Rise, Weddel Sea, Paleoceanography, 17, 1029–1042, doi:10.1029/2001PA000662, 2002.

CPD
11, 4329–4389, 2015

Bralower, T. J. and Mutterlose, J.: Calcareous nannofossil biostratigraphy of ODP Site 865, Allison Guyot, Central Pacific Ocean: a tropical Paleogene reference section, Proc. Ocean Drill. Prog. Sci. Results, 143, 31–72, 1995.

Bukry, D.: Low-latitude coccolith biostratigraphic zonation, Initial Rep. Deep Sea, 15, 685–703, 1973.

Cati, A., Sartorio, D., and Venturini, S.: Carbonate Platforms in the Subsurface of the Northern Adriatic Area, Memorie della Società Geologica Italiana, 40, 295–308, 1989.

Corfield, R. M.: Palaeocene oceans and climate: an isotopic perspective, Earth Sci. Rev., 37, 225–252, doi:10.1016/0012-8252(94)90030-2, 1994.

Costa, V., Doglioni, C., Grandesso, P., Masetti, D., Pellegrini, G. B., and Tracanella, E.: Carta Geologica d'Italia, Foglio 063, Belluno: Roma, Servizio Geologico d'Italia, scale 1 : 50000, 1 sheet + 74 p., 1996.

Cramer, B. S., Wright, J. D., Kent, D. V., and Aubry, M.-P.: Orbital climate forcing of δ^{13}C excursions in the late Paleocene–early Eocene (Chrons C24n–C25n), Paleoceanography, 18, 1097, doi:10.1029/2003PA000909, 2003.

Cramer, B. S., Toggweiler, J. R., Wright, J. D., Katz, M. E., and Miller, K. G.: Ocean overturning since the Late Cretaceous: inferences from a new benthic foraminiferal isotope compilation, Paleoceanography, 24, PA4216, doi:10.1029/2008PA001683, 2009.

Dallanave, E., Agnini, C., Muttoni, G., and Rio, D.: Magneto-biostratigraphy of the Cicogna section (Italy): implications for the late Paleocene-early Eocene time scale, Earth Planet. Sc. Lett., 285, 39–51, doi:10.1016/j.epsl.2009.05.033, 2009.

Dallanave, E., Agnini, C., Bachtadse, V., Muttoni, G., Crampton, J. S., Strong, C. P., Hines, B. R., Hollis, C. J., and Slotnick., B. S.: Early to middle Eocene magnetostratigraphy of the southwest Pacific Ocean and climate influence on sedimentation: insights from the Mead Stream section, New Zealand, Geol. Soc. Am. Bull., 127, 643–660, 2015.

DeConto, R. M., Galeotti, S., Pagani, M., Tracy, D., Schaefer, K. Zhang, T., Pollard, D., and Beerling, D. J.: Past extreme warming events linked to massive carbon release from thawing permafrost, Nature, 484, 87–91, doi:10.1038/nature10929, 2012.

Dickens, G. R.: Rethinking the global carbon cycle with a large, dynamic and microbially mediated gas hydrate capacitor, Earth Planet. Sc. Lett., 213, 169–183, 2003.

Dickens, G. R. and Backman, J.: Core alignment and composite depth scale for the lower Paleogene through uppermost Cretaceous interval at Deep Sea Drilling Project Site 577, Newslett. Stratigr., 46, 47–68, doi:10.1127/0078-0421/2013/0027, 2013.

CPD
11, 4329–4389, 2015

Dickens, G. R., Castillo, M. M., and Walker, J. C. G.: A blast of gas in the latest Paleocene: simulating first-order effects of massive dissociation of oceanic methane hydrate, Geology, 25, 259–262, 1997.

Doglioni, C. and Bosellini, A.: Eoalpine and mesoalpine tectonics in the Southern Alps, Geol. Rundsch., 77, 734–754, 1987.

Dupuis, C., Aubry, M.-P., Steurbaut, E., Berggren, W. A., Ouda, K., Magioncalda, R., Cramer, B. S., Kent, D. V., Speijer, R. P., and Heilmann-Clausen, C.: The Dababiya Quarry section: lithostratigraphy, geochemistry and paleontology, Micropaleontology, 49, 41–59, 2003.

Erba, E., Bottini, C., Weissert, H. J., and Keller, C. E.: Calcareous nannoplankton response to surface-water acidification around Oceanic Anoxic Event 1a, Science, 329, 428, doi:10.1126/science.1188886, 2010.

Frank, T. D., Arthur, M. A., and Dean, W. E.: Diagenesis of Lower Cretaceous pelagic carbonates, North Atlantic: paleoceanographic signals obscured, J. Foramin. Res., 29, 340–351, 1999.

Geisen, M., Young, J. R., Probert, I., Sáez, A. G., Baumann, K.-H., Bollmann, J., Cros, L., De Vargas, C., Medlin, L. K., and Sprengel, C.: Species level variation in coccolithophores, in: Coccolithophores – From Molecular Processes to Global Impact, Springer, Berlin, 327–366, 2004.

Gibbs, S. J., Shackleton, N. J., and Young, J. R.: Orbitally forced climate signals in mid-Pliocene nannofossil assemblages, Mar. Micropaleontol., 51, 39–56, 2004.

Gibbs, S. J., Bown, P. R., Sessa, J. A., Bralower, T. J., and Wilson, P. A.: Nannoplankton extinction and origination across the Paleocene-Eocene thermal maximum, Science, 314, 1770–1773, doi:10.1126/science.1133902, 2006a.

Gibbs, S. J., Bralower, T. J., Bown, P. R., Zachos, J. C., and Bybell, L. M.: Shelf and open-ocean calcareous phytoplankton assemblages across the Paleocene–Eocene thermal maximum: implications for global productivity gradients, Geology, 34, 233–236, doi:10.1130/G22381.1, 2006b.

Gibbs, S. J., Bown, P. R., Murphy, B. H., Sluijs, A., Edgar, K. M., Pälike, H., Bolton, C. T., and Zachos, J. C.: Scaled biotic disruption during early Eocene global warming events, Biogeosciences, 9, 4679–4688, doi:10.5194/bg-9-4679-2012, 2012.

CPD
11, 4329–4389, 2015

Giusberti, L., Rio, D., Agnini, C., Backman, J., Fornaciari, E., Tateo, F., and Oddone, M.: Mode and tempo of the Paleocene-Eocene Thermal Maximum in an expanded section in the Venetian Pre-Alps, Geol. Soc. Am. Bull., 119, 391–412, doi:10.1130/B25994.1, 2007.

Gradstein, F. M., Ogg, J. G., Schmitz, M. D., and Ogg, G. M. (Eds.): The Geological Time Scale 2012, Elsevier, Amsterdam, 2012.

Grandesso, P.: Biostratigrafia delle formazioni terziarie del Vallone Bellunese, Boll. Soc. Geol. Ital., 94, 1323–1348, 1976.

Hammer, Ø, Harper, D. A. T., and Ryan, P. D.: PAST: Paleontological Statistics Software package for education and data analysis, Palaeontol. Electron., 4, 19–20, 2001.

Haq, B. U. and Lohmann, G. P.: Early Cenozoic calcareous nannoplankton biogeography of the Atlantic Ocean, Mar. Micropaleontol., 1, 119–194, 1976.

Hay, W. W.: Carbonate fluxes and calcareous nannoplankton, in: Coccolithophores – From Molecular Processes to Global Impact, Springer, Berlin, 508–528, 2004.

Hönisch, B., Ridgwell, A., Schmidt, D. N., Thomas, E., Gibbs, S. J., Sluijs, A., Zeebe, R., Kump, L., Martindale, R. C., Greene, S. E., Kiessling, W., Ries, J., Zachos, J. C., Royer, D. L., Barker, S., Marchitto Jr., T. M., Moyer, R., Pelejero, C., Ziveri, P., Foster, G. L., and Williams, B.: The geological record of ocean acidification, Science, 335, 1058–1063, doi:10.1126/science.1208277, 2012.

Hollis, C. J., Taylor, K. W. R., Handley, L., Pancost, R. D., Huber, M., Creech, J. B., Hines, B. R., Crouch, E. M., Morgans, H. E. G., Crampton, J. S., Gibbs, S., Pearson, P. N., and Zachos, J. C.: Early Paleogene temperature history of the Southwest Pacific Ocean: reconciling proxies and models, Earth Planet. Sc. Lett., 349, 53–66, 2012.

Huber, M. and Caballero, R.: The early Eocene equable climate problem revisited, Clim. Past, 7, 603–633, doi:10.5194/cp-7-603-2011, 2011.

Iglesias-Rodriguez, M. D., Halloran, P. R., Rickaby, R. E. M., Hall, I. R., Colmenero-Hidalgo, E., Gittins, J. R., Green, D. R. H., Tyrrell, T., Gibbs, S. J., Von Dassow, P., Rehm, E., Armbrust, E. V., and Boessenkool, K. P.: Phytoplankton calcification in a high-CO_2 world, Science, 320, 336–340, doi:10.1126/science.1154122, 2008.

Jiang, S. and Wise Jr., S. W.: Distinguishing the influence of diagenesis on the paleoecological reconstruction of nannoplankton across the Paleocene/Eocene Thermal Maximum: an example from the Kerguelen Plateau, southern Indian Ocean, Mar. Micropaleontol., 72, 49–59, doi:10.1016/j.marmicro.2009.03.003, 2009.

CPD
11, 4329–4389, 2015

Keeling, C. D. and Whorf, T. P.: Atmospheric carbon dioxide record from Mauna Loa, in: Oak Ridge Laboratory Trends: a Compendium of Data on Global Change, Carbon Dioxide Information Analysis Center, Oak Ridge National Laboratory, U.S. Department of Energy, Oak Ridge, Tennessee, USA, doi:10.3334/CDIAC/atg.ndp001.2004, 2004.

Kirtland-Turner, S., Sexton, P. F., Charles, C. D., and Norris, R. D.: Persistence of carbon release events through the peak of early Eocene global warmth, Nat. Geosci., 7, 748–751, doi:10.1038/ngeo2240, 2014.

Kleypas, J. A., Feely, R. A., Fabry, V. J., Langdon, C., Sabine, C. L., and Robbins, L. L.: Impacts of Ocean Acidification on Coral Reefs and Other Marine Calcifiers: a Guide For Future Research, Contrib. No. 2857, NOAA/Pacific Marine Environm. Lab., 88 pp., 2006.

Komar, N., Zeebe, R. E., and Dickens, G. R.: Understanding long-term carbon cycle trends: the late Paleocene through the early Eocene, Paleoceanography, 28, 650–662, doi:10.1002/palo.20060, 2013.

Krishnan, S., Pagani, M., Agnini, C.: Leaf waxes as recorders of paleoclimatic changes during the Paleocene-Eocene Thermal Maximum: regional expressions from the Belluno Basin, Org. Geochem., 80, 8–17, doi:10.1016/j.orggeochem.2014.12.005, 2015.

Kroopnick, P. M.: The distribution of ^{13}C of ΣCO_2 in the world oceans, Deep-Sea Res., 32, 57–84, 1985.

Kump, L. R., Bralower, T. J., and Ridgwell, A.: Ocean acidification in deep time, Oceanography, 22, 94–107, 2009.

Kurtz, A. C., Kump, L. R., Arthur, M. A., Zachos, J. C., and Paytan, A.: Early Cenozoic decoupling of the global carbon and sulfur cycles, Paleoceanography, 18, 1090, doi:10.1029/2003PA000908, 2003.

Langer, G., M., Geisen, Baumann, K.-H., Kläs, J., Riebesell, U., Thoms, S., and Young, J. R.: Species-specific response of calcifying algae to changing seawater carbonate chemistry, Geochem. Geophy. Geosy., 7, Q09006, doi:10.1029/2005GC001227, 2006.

Leon-Rodriguez, L. and Dickens, G. R.: Constraints on ocean acidification associated with rapid and massive carbon injections: the early Paleogene record at Ocean Drilling Program Site 1215, Equatorial Pacific Ocean, Palaeogeogr. Palaeocl., 298, 409–420, doi:10.1016/j.palaeo.2010.10.029, 2010.

Lohbeck, K. T., Riebesell, U., and Reusch, T. B. H.: Adaptive evolution of a key phytoplankton species to ocean acidification, Nat. Geosci., 5, 346–351, doi:10.1038/ngeo1441, 2012.

CPD
11, 4329–4389, 2015

Lourens, L. J., Sluijs, A., Kroon, D., Zachos, J. C., Thomas, E., Röhl, U., Bowles, J., and Raffi, I.: Astronomical pacing of late Palaeocene to early Eocene global warming events, Nature, 435, 1083–1087, doi:10.1038/nature03814, 2005.

Lunt, D. J., Ridgwell, A., Sluijs, A., Zachos, J. C., Hunter, S., and Haywood, A.: A model for orbital pacing of methane hydrate destabilization during the Palaeogene, Nat. Geosci., 4, 775–778, doi:10.1038/ngeo1266, 2011.

MacArthur, R. and Wilson, E. O.: The Theory of Island Biogeography, Princeton University Press, ISBN 0-691-08836-5M, 1967.

Marino, M., Maiorano, P., and Lirer, F.: Changxes in calcareous nannofossil assemblages during the Mid-Pleistocene Revolution, Mar. Micropaleontol., 69, 70–90, doi:10.1016/j.marmicro.2007.11.010, 2008.

Marshall, J. D.: Climatic and oceanographic isotopic signals from the carbonate rock record and their preservation, Geol. Mag., 129, 143–160, doi:10.1017/S0016756800008244, 1992.

Martini, E.: Standard Tertiary and Quaternary calcareous nannoplankton zonation, in: Proceedings of the 2nd Planktonic Conference, 2, Tecnoscienza, Roma, 739–785, 1971.

Matter, A., Douglas, R. G., and Perch-Nielsen, K: Fossil preservation, geochemistry and diagenesis of pelagic carbonates from Shatsky Rise, northwest Pacific, Initial Rep. Deep Sea, 32, 891–922, 1975.

Miller, K. G., Fairbanks, R. G., and Mountain, G. S.: Tertiary oxygen isotope synthesis, sea level history, and continental margin erosion, Paleoceanography, 2, 1–19, doi:10.1029/PA002i001p00001, 1987.

Milliman, J. D.: Production and accumulation of calcium carbonate in the ocean: budget of a nonsteady state, Global Biogeochem. Cy., 7, 927–957, doi:10.1029/93GB02524, 1993.

Monechi, S., Angori, E., von Salis, K.: Calcareous nannofossil turnover around the Paleocene/Eocene transition at Alamedilla (southern Spain), Bull. Soc. Geol. Fr., 171, 477–489, 2000.

Mutterlose, J., Linnert, C., and Norris, R.: Calcareous nannofossils from the Paleocene-Eocene Thermal Maximum of the equatorial Atlantic (ODP Site 1260B): evidence for tropical warming, Mar. Micropaleontol., 65, 13–31, doi:10.1016/j.marmicro.2007.05.004, 2007.

Nicolo, M. J., Dickens, G. R., Hollis, C. J., and Zachos, J. C.: Multiple early Eocene hyperthermals: their sedimentary expression on the New Zealand continental margin and in the deep sea, Geology, 35, 699–702, doi:10.1130/G23648A.1, 2007.

CPD
11, 4329–4389, 2015

Norris, R. D., Wilson, P. A., and Blum, P., and the Expedition 342 Scientists: Expedition 342 summary, Proc. IODP, 342, 1–149, doi:10.2204/iodp.proc.342.2014, 2014.
Ogg, J. G.: Geomagnetic polarity time scale, in: The Geologica Time Scale 2012, edited by: Gradstein, F. M., Ogg, J. G., Schmitz, M. D., and Ogg, G. M., Elsevier, Amsterdam, the Netherlands, 85–113, 2012.
Ogg, J. G. and Bardot, L.: Aptian through Eocene magnetostratigraphic correlation of the Blake Nose Transect (Leg 171B), Florida continental margin, in: Proc. ODP, Sci. Results, edited by: Kroon, D., Norris, R. D., and Klaus, A., Proc. ODP, Sci. Results B, 171, 1–58, 2001.
Ogg, J. G. and Smith, A. G.: The geomagnetic polarity time scale, in: A Geological Timescale 2004, edited by: Gradstein, F., Ogg, J. G., and Smith, A., Cambridge Univ. Press, Cambridge, UK, 63–86, 2004.
Okada, H. and Bukry, D.: Supplementary modification and introduction of code numbers to the low-latitude coccolith biostratigraphic zonation (Bukry, 1973; 1975), Mar. Micropaleontol., 5, 321–325, doi:10.1016/0377-8398(80)90016-X, 1980.
Pälike, H., Lyle, M. W., Nishi, H., Raffi, I., Ridgwell, A., Gamage, K., Klaus, A., Acton, G. D., Anderson, L., Backman, J., Baldauf, J. G., Beltran, C., Bohaty, S. M., Bown, P. R., Busch, W. H., Channell, J. E. T., Chun, C. O. J., Delaney, M. L., Dewang, P., Dunkley Jones, T., Edgar, K. M., Evans, H. F., Fitch, P., Foster, G. L., Gussone, N., Hasegawa, H., Hathorne, E. C., Hayashi, H., Herrle, J. O., Holbourn, A. E. L., Hovan, S. A., Hyeong, K., Iijima, K., Ito, T., Kamikuri, S.-I., Kimoto, K., Kuroda, J., Leon-Rodriguez, L., Malinverno, A., Moore, T. C., Murphy, B., Murphy, D. P., Nakamura, H., Ogane, K., Ohneiser, C., Richter, C., Robinson, R. S., Rohling, E. J., Romero, O. E., Sawada, K., Scher, H. D., Schneider, L., Sluijs, A., Takata, H., Tian, J., Tsujimoto, A., Wade, B. S., Westerhold, T., Wilkens, R. H., Williams, T., Wilson, P. A., Yamamoto, Y., Yamamoto, S., Yamazaki, T., and Zeebe, R. E.: A Cenozoic record of the equatorial Pacific carbonate compensation depth, Nature, 488, 609–614, doi:10.1038/nature11360, 2012.
Payros, A., Ortiz, S., Millán, I., Arostegi, J., Orue-Etxebarria, X., and Apellaniz, E.: Early Eocene climatic optimum: environmental impact on the North Iberian continental margin, Geol. Soc. Am. Bull., doi:10.1130/B31278.1, in press, 2015.
Pearson, P. N., van Dongen, B. E., Nicholas, C. J., Pancost, R. D., Schouten, S., Singano, J. M., and Wade, B. S.: Stable warm tropical climate through the Eocene Epoch, Geology, 35, 211–214, 2007.

CPD
11, 4329–4389, 2015

Perch-Nielsen, K.: Cenozoic calcareous nannofossils, in: Plankton Stratigraphy, Cambridge Univ. Press, New York, 427–554, 1985.
Pianka, E. R.: On *r* and *K* selection, Amer. Natural., 104, 592–597, doi:10.1086/282697, 1970.
Premoli Silva, I. and Sliter, W. V.: Cretaceous paleoceanography: evidence from planktonic foraminiferal evolution, Geol. Soc. Am. Spec. Pap., 332, 301–328, doi:10.1130/0-8137-2332-9.301, 1999.
Raffi, I. and De Bernardi, B.: Response of calcareous nannofossils to the Paleocene-Eocene Thermal Maximum: observations on composition, preservation and calcification in sediments from ODP Site 1263 (Walvis Ridge – SW Atlantic), Mar. Micropaleontol., 69, 119–138, doi:10.1016/j.marmicro.2008.07.002, 2008.
Raffi, I., Backman, J., and Pälike, H.: Changes in calcareous nannofossil assemblage across the Paleocene/Eocene transition from the paleo-equatorial Pacific Ocean, Palaeogeogr. Palaeocl., 226, 93–126, doi:10.1016/j.palaeo.2005.05.006, 2005.
Raffi, I., Backman, J., Zachos, J. C., Sluijs, A.: The response of calcareous nannofossil assemblages to the Paleocene Eocene Thermal Maximum at the Walvis Ridge in the South Atlantic, Mar. Micropaleontol., 70, 201–212, 2009.
Raven, J., Caldeira, K., Elderfield, H., Hoegh-Guldberg, O., Liss, P., Riebesell, U., Shepherd, J., Turley, C., and Watson, A.: Ocean Acidification Due to Increasing Atmospheric Carbon Dioxide, Royal Society Policy Document 12/05, ISBN 0 85403 617 2, London, 60 pp., 2005.
Riebesell, U., Zondervan, I., Rost, B., Tortell, P. D., Zeebe, R. E., and Morel, F. M. M.: Reduced calcification of marine plankton in response to increased atmospheric CO_2, Nature, 407, 364–367, doi:10.1038/35030078, 2000.
Riebesell, U., Bellerby, R. G. J., Engel, A., Fabry, V. J., Hutchins, D. A., Reusch, K. G., Schulz, T. B. H., and Morel, F. M. M.: Comment on "Phytoplankton calcification in a high-CO2 world", Science, 322, 1466b, doi:10.1126/science.1161096, 2008.
Romein, A. J. T.: Lineages in early Paleogene calcareous nannoplankton, Utrecht Micropaleont. Bull., 22, 1–231, 1979.
Rost, B. and Riebesell, U.: Coccolithophores and the biological pump: responses to environmental changes, in: Coccolithophores – From Molecular Processes to Global Impact, Springer, Berlin, 99–125, 2004.
Roth, P. H.: Jurassic and lower Cretaceous calcareous nannofossils in the western North Atlantic (Site 534): biostratigraphy, preservation, and some observations on biogeography and

CPD
11, 4329–4389, 2015

paleoceanography, in: DSDP Init. Repts., edited by: Sheridan, R. E., Gradstein, F. M. et al., DSDP Init. Repts., 76, 587–621, 1983.
Roth, P. H. and Thierstein, H. R.: Calcareous nannoplankton: Leg XIV of the Deep Sea Drilling Project, in: DSDP Init. Repts., edited by: Hayes, D. E., Pimm, A. C., et al., DSDP Init. Repts., 14, 421–486, 1972.
Schrag, D. P., DePaolo, D. J., and Richter, F. M.: Reconstructing past sea surface temperatures: correcting for diagenesis of bulk marine carbonate, Geochim. Cosmochim. Ac., 59, 2265–2278, 1995.
Scholle, P. A. and Arthur, M. A.: Carbon isotope fluctuations in Cretaceous pelagic limestones: potential stratigraphic and petroleum exploration tool, Amer. Assoc. Pet. Geol. Bull., 64, 67–87, 1980.
Self-Trail, J. M., Powars, D. S., Watkins, D. K., and Wandless, G.: Calcareous nannofossil assemblage changes across the Paleocene-Eocene thermal maximum: evidence from a shelf setting, Mar. Micropaleontol., 92/93, 61–80, doi:10.1016/j.marmicro.2012.05.003, 2012.
Shackleton, N. J.: Paleogene stable isotope events, Palaeogeogr. Palaeocl., 57, 91–102, 1986.
Shamrock, J. L.: Eocene Calcareous Nannofossil Biostratigraphy, Paleoecology and Biochronology of ODP Leg 122 Hole 762c, Eastern Indian Ocean (Exmouth Plateau), Ph.D. thesis, University of Nebraska, Nebraska, 2010.
Slotnick, B. S., Dickens, G. R., Nicolo, M. J., Hollis, C. J., Crampton, J. S., Zachos, J. C., and Sluijs, A.: Large-amplitdue variations in carbon cycling and terrestrial weathering during the latest Paleocene and earliest Eocene: the record at Mead Stream, New Zealand, J. Geol., 120, 1–19, doi:10.1086/666743, 2012.
Slotnick, B. S., Lauretano, V., Backman, J., Dickens, G. R., Sluijs, A., and Lourens, L.: Early Paleogene variations in the calcite compensation depth: new constraints using old borehole sediments from across Ninetyeast Ridge, central Indian Ocean, Clim. Past, 11, 473–493, doi:10.5194/cp-11-473-2015, 2015a.
Slotnick, B. S., Dickens, G. R., Hollis, C. J., Crampton, J. S., Strong, C. P., and Phillips, A.: The onset of the Early Eocene Climatic Optimum at Branch Stream, Clarence River valley, New Zealand, New Zealand J. Geol. Geophys., in press, 2015b.
Spofforth, D. J. A., Agnini, C., Pälike, H., Rio, D., Fornaciari, E., Giusberti, L., Luciani, V., Lanci, L., Muttoni, G., and Bohaty, S. M.: Organic carbon burial following the Middle Eocene Climatic Optimum (MECO) in the central – western Tethys, Paleoceanography, 25, PA3210, doi:10.1029/2009PA001738, 2010.

CPD
11, 4329–4389, 2015

Stefani, C. and Grandesso, P.: Studio preliminare di due sezioni del Flysch bellunese, Rend. Soc. Geol. It., 14, 157–162, 1991.
Stillman, J. H. and Paganini, A. W.: Biogeochemical adaptation to ocean acidifcation, J. Exp. Biol., 218, 1946–1955, doi:10.1242/jeb.115584, 2015.
Stoll, H. M. and Bains, S.: Coccolith Sr/Ca records of productivity during the Paleocene-Eocene thermal maximum from the Weddell Sea, Paleoceanography, 18, 1049, doi:10.1029/2002PA000875, 2003.
Tagliabue, A. and Bopp, L.: Towards understanding global variability in ocean carbon-13, Global Biogeochem. Cy., 22, GB1035, doi:10.1029/2007GB003037, 2008.
Thierstein, H., Geitzenauer, K. R., Molfino, B., and Shackleton, N. J.: Global synchroneity of late Quaternary coccolith datum levels: validation by oxygen isotopes, Geology, 5, 400–404, 1977.
Thibault, N. and Gardin, S.: The calcareous nannofossil response to the end-Cretaceous warm event in the tropical Pacific, Palaeogeogr. Palaeocl., 291, 239–252, doi:10.1016/j.palaeo.2010.02.036, 2010.
Tipple, B. J., Pagani, M., Krishnan, S., Dirghangi, S. S., Galeotti, S., Agnini, C., Giusberti, L., and Rio, D.: Coupled high-resolution marine and terrestrial records of carbon and hydrologic cycles variations during the Paleocene-Eocene Thermal Maximum (PETM), Earth Planet. Sc. Lett., 311, 82–92, doi:10.1016/j.epsl.2011.08.045, 2011.
Toffanin, F., Agnini, C., Fornaciari, E., Rio, D., Giusberti, L., Luciani, V., Spofforth, D. J. A., and Pälike, H.: Changes in calcareous nannofossil assemblages during the Middle Eocene Climatic Optimum: clues from the central-western Tethys (Alano section, NE Italy), Mar. Micropaleontol., 81, 22–31, doi:10.1016/j.marmicro.2011.07.002, 2011.
Toffanin, F., Agnini, C., Rio, D., Acton, G., and Westerhold, T.: Middle Eocene to Early Oligocene calcareous nannofossil biostratigraphy at Site U1333c (Pacific Equatorial), Micropaleontology, 59, 69–82, 2013.
Tremolada, F. and Bralower, T. J.: Nannofossil assemblage fluctuations during the Paleocene–Eocene Thermal Maximum at Sites 213 (Indian Ocean) and 401 (North Atlantic Ocean): palaeoceanographic implications, Mar. Micropaleontol., 52, 107–116, doi:10.1016/j.marmicro.2004.04.002, 2004.
Vandenberghe, N., Hilgen, F. J., and Speijer, R. P.: The Paleogene Period, in: The Geologic Time Scale 2012, edited by: Gradstein, F., Ogg, J., Schmitz, M., and Ogg, G., Elsevier, Amsterdam, the Netherlands, 855–922, 2012.

CPD
11, 4329–4389, 2015

Watkins, D. K. and Self-Trail, J. M.: Calcareous nannofossil evidence for the existence of the Gulf Stream during the late Maastrichtian, Paleoceanography, 20, Pa3006, doi:10.1029/2004pa001121, 1992.

Wei, W. and Wise Jr. S. W.: Biogeographic gradients of middle Eocene–Oligocene calcareous nannoplankton in the South Atlantic Ocean, Palaeogeogr. Palaeocl., 79, 29–61, 1990.

Westerhold, T., Röhl, U., Raffi, I., Fornaciari, E., Monechi, S., Reale, V., Bowles, J., and Evans, H. F.: Astronomical calibration of the Paleocene time, Palaeogeogr. Palaeocl., 257, 377–403, doi:10.1016/j.palaeo.2007.09.016, 2008.

Westerhold, T., Röhl, U., Donner, B., McCarren, H. K., and Zachos, J. C.: A complete high – resolution Paleocene benthic stable isotope record for the central Pacific (ODP Site 1209), Paleoceanography, 26, PA2216, doi:10.1029/2010PA002092, 2011.

Winter, A., Jordan, R. W., and Roth, P. H.: Biogeography of living coccolithophores, in: Coccolithophores, edited by: Winter, A. and Siesser, W. G., Cambridge Univ. Press, Cambridge (UK), 161–177, 1994.

Winterer, E. L. and Bosellini, A.: Subsidence and sedimentation on Jurassic passive continental margin, Southern Alps, Italy, Am. Assoc. Petr. Geol. Bull., 65, 394–421, 1981.

Young, J. R., Geisen, M., and Probert, I.: A review of selected aspects of coccolithophore biology with implications for paleobiodiversity estimation, Micropaleontology, 51, 267–288, 2005.

Zachos, J. C., Kroon, D., Blum, P., Bowles, J., Gaillot, P., Hasegawa, T., Hathorne, E. C., Hodell, D. A., Kelly, D. C., Jung, J.-H., Keller, S. M., Lee, Y.S., Leuschner, D. C., Liu, Z., Lohmann, K. C., Lourens, L. J., Monechi, S., Nicolo, M., Raffi, I. Riesselman, C., Röhl, U., Schellenberg, S. A., Schmidt, D., Sluijs, A., Thomas, D., Thomas, E., and Vallius H.: Early Cenozoic Extreme Climates: the Walvis Ridge Transect, Proc. Ocean Drill. Program, Initial Rep. 208, available at: http://www-odp.tamu.edu/publications/208_IR/208ir.htm, 2004.

Zachos, J. C., Röhl, U., Schellenberg, S. A., Sluijs, A., Hodell, D. A., Kelly, D. C., Thomas, E., Nicolo, M., Raffi, I., Lourens, L. J., McCarren, H., and Kroon, D.: Rapid acidification of the ocean during the Paleocene-Eocene Thermal Maximum, Science, 308, 1611–1615, doi:10.1126/science.1109004, 2005.

Zachos, J. C., Dickens, G. R., and Zeebe, R. E.: An early Cenozoic perspective on greenhouse warming and carbon-cycle dynamics, Nature, 451, 279–283, doi:10.1038/nature06588, 2008.

CPD
11, 4329–4389, 2015

Zachos, J. C., McCarren, H., Murphy, B., Röhl, U., and Westerhold, T.: Tempo and scale of late Paleocene and early Eocene carbon isotope cycles: implications for the origin of hyperthermals, Earth Planet. Sc. Lett., 299, 242–249, doi:10.1016/j.epsl.2010.09.004, 2010.

Zattin, M., Cuman, A., Fantoni, R., Martin, S., Scotti, P., and Stefani, C.: From middle Jurassic heating to Neogene cooling: the thermochronological evolution of the southern Alps, Tectonophysics, 414, 191–202, doi:10.1016/j.tecto.2005.10.020, 2006.

Zeebe, R. E. and Westbroek, P.: A simple model for the $CaCO_3$ saturation state of the ocean: the "Strangelove", the "Neritan", and the "Cretan" ocean, Geochem. Geophy. Geosy., 4, 1104, doi:10.1029/2003GC000538, 2003, 2003.

Zeebe, R. E., Zachos, J. C., and Dickens, G. R.: Carbon dioxide forcing alone insufficient to explain Paleocene-Eocene Thermal Maximum warming, Nat. Geosci., 2, 576–580, doi:10.1038/NGEO578, 2009.

Ziveri, P., Young, J., and van Hinte, J. E.: Coccolithophore export production and accumulation rates, in: On Determination of Sediment Accumulation Rates, GeoResearch Forum, Trans Tech Publications LTD, Switzerland, 5, 41–56, 1999.

CPD
11, 4329–4389, 2015

Table 1. Heights and ages of polarity chron boundaries, key calcareous nannofossil datums, and CIEs at the Cicogna Section and ODP Site 1262.

Event		Nanno Zones			Cicogna section		DAMR09[d]		W01	CK95	GTS04	GTS12
		NP[a]	CP[b]	CN[c]	Height (m)	Err (m)	Chron notation		Age (Ma)	Age (Ma)	Age (Ma)	Age (Ma)
	C23r base				77.94			0.000	52.364	52.364	52.648	52.620
	K-X base				72.20	0.10	C24n.1n	0.786	52.57	52.60	52.93	52.98
B	*Discoaster lodoensis*	NP12	CP10		71.10	0.10	C24n.1n	0.936	52.61	52.64	52.98	53.05
Bc	*Chiprhagmalithus* spp.				71.10	0.10	C24n.1n	0.936	52.61	52.64	52.98	53.05
	C24n.1n base				70.64			0.000	52.630	52.663	53.004	53.074
	C24n.1r base				68.80			0.000	–	52.757	53.116	53.199
	C24n.2n base				68.21			0.000	–	52.801	53.167	53.274
B	*Chiprhagmalithus* spp.				66.50	0.50	C24n.2r	0.473	52.82	52.85	53.22	53.34
	J base				65.40	0.10	C24n.2r	0.778	52.94	52.88	53.26	53.38
	C24n.2r base				64.60			0.000	53.030	52.903	53.286	53.416
B	*Girgisia gammation*				61.20	0.10	C24n.3n	0.526	53.29	53.14	53.56	53.71
Br	*Discoaster lodoensis*				60.40	0.10	C24n.3n	0.650	53.36	53.19	53.63	53.78
T	*Discoaster multiradiatus*				60.20	0.10	C24n.3n	0.681	53.37	53.21	53.64	53.80
	I1/I2 base				60.10	0.10	C24n.3n	0.697	53.38	53.21	53.65	53.81
	C24n.3n base				58.14			0.000	55.530	53.347	53.808	53.983
	H1-Elmo/H2 base				53.90	0.10	C24r	0.090	53.81	53.58	54.06	54.26
T	*Tribrachiatus contortus*	NP11	CP9b		52.70	0.10	C24r	0.115	53.89	53.64	54.14	54.34
Tc	*Discoaster multiradiatus*				51.50	0.10	C24r	0.141	53.97	53.71	54.21	54.42
B	*Sphenolithus radians*				51.30	0.10	C24r	0.145	53.98	53.72	54.22	54.43
B	*Tribrachiatus orthostylus*			CNE3	51.30	0.10	C24r	0.145	53.98	53.72	54.22	54.43
T	*Tribrachiatus bramlettei*				48.50	0.50	C24r	0.204	54.17	53.87	54.39	54.62
B	*Tribrachiatus contortus*		CP9a		45.50	0.50	C24r	0.268	54.37	54.03	54.57	54.82
B	*Discoaster diastypus*		CP9a		42.70	0.10	C24r	0.327	54.55	54.18	54.74	55.00
B	*Tribrachiatus bramlettei*	NP10			35.58	0.55	C24r	0.478	55.03	54.57	55.17	55.47
T	*Fasciculithus* spp./*F. tympaniformis*			CNE2	34.73	0.13	C24r	0.496	55.08	54.61	55.22	55.53
T	*Rhomboaster* spp.				32.52	0.48	C24r	0.543	55.23	54.73	55.36	55.67

CPD
11, 4329–4389, 2015

Table 1. Continued.

Event		Nanno Zones			Cicogna section		DAMR09[d]		W01	CK95	GTS04	GTS12
		NP[a]	CP[b]	CN[c]	Height (m)	Err (m)	Chron notation		Age (Ma)	Age (Ma)	Age (Ma)	Age (Ma)
X	*Fasciculithus/Zygrhablithus*				31.60	0.10	C24r	0.562	55.29	54.78	55.41	55.74
Br	*Tribrachiatus bramlet-tei*				29.43	0.18	C24r	0.608	55.43	54.90	55.55	55.88
B	*Discoaster araneus*				28.95	0.05	C24r	0.618	55.47	54.93	55.57	55.91
B	*Rhomboaster* spp.	NP9b	CP8b		28.88	0.03	C24r	0.620	55.47	54.93	55.58	55.92
	PETM				28.73	0.03	C24r	0.623	55.48	54.94	55.59	55.93
	P/E boundary (extrap-olated)				28.73	0.03	C24r	0.623	55.48	54.94	55.59	55.93
decrease	*Fasciculithus* spp.				28.73	0.03	C24r	0.623	55.48	54.94	55.59	55.93
T	*F. richardii* gr.			CNE1	28.73	0.03	C24r	0.623	55.48	54.94	55.59	55.93
	? base				25.00	0.10	C24r	0.702	55.73	55.14	55.81	56.17
	D1/D2 base				20.00	0.10	C24r	0.808	56.06	55.41	56.12	56.50
	C1/C2 base				12.61	0.10	C24r	0.964	56.55	55.81	56.56	56.99
T	*Ericsonia robusta*				11.2	0.2	C24r	0.994	56.64	55.89	56.65	57.08
	C24r base				10.93			0.000	56.660	55.904	56.665	57.101
Bc	*F. alanii*				10.51	0.49	C25n	0.060	56.69	55.93	56.70	57.13
B	*Discoaster multiradia-tus*	NP9a			9.90	0.10	C25n	0.147	56.74	55.98	56.74	57.18
Tc	*Sphenolithus anarrho-pus*				8.62	0.49	C25n	0.331	56.84	56.07	56.84	57.28
B	*Discoaster delicatus* gr.				6.86	0.12	C25n	0.583	56.97	56.19	56.97	57.42
	B1/B2 base				5.41	0.10	C25n	0.791	57.08	56.29	57.07	57.54
B	*Ericsonia robusta*				3.97	0.07	C25n	0.998	57.20	56.39	57.18	57.65
	C25n base				3.96			0.000	57.197	56.391	57.180	57.656
B	*Discoaster nobilis* gr.		CP7		2.14	0.05	C25r		57.337	56.518	57.314	57.801
B	*D. mohleri*	NP7	CP6		–	–	–	–	–	–	–	–
	C25r base				–			0.000	58.550	57.554	58.379	58.959

CPD
11, 4329–4389, 2015

Table 1. Continued.

Event		Site 1262 Depth (mcd)	Err (m)	AG07[e]/This study Chron notation		W01 Age (Ma)	CK95 Age (Ma)	GTS04 Age (Ma)	GTS12 Age (Ma)
	C23r base	105.88			0.000	52.364	52.364	52.648	52.620
	K-X base	–	–	–	–	–	–	–	–
B	*Discoaster lodoensis*	107.67	0.18	C24n.1n	0.777	52.57	52.60	52.92	52.97
Bc	*Chiprhagmalithus* spp.	107.67	0.18	C24n.1n	0.777	52.57	52.60	52.92	52.97
	C24n.1n base	108.19			0.000	52.630	52.663	53.004	53.074
	C24n.1r base	–			0.000	–	52.757	53.116	53.199
	C24n.2n base	–			0.000	–	52.801	53.167	53.274
B	*Chiprhagmalithus* spp.	109.22	0.10	C24n.2r/.1r	0.358	52.77	52.75	53.11	53.20
	J base	109.96	0.02	C24n.2r/.1r	0.616	52.88	52.81	53.18	53.28
	C24n.2r base	111.06			0.000	53.03	52.903	53.286	53.416
B	*Girgisia gammation*	113.52	0.11	C24n.3n	0.540	53.30	53.14	53.57	53.72
Br	*Discoaster lodoensis*	113.52	0.11	C24n.3n	0.540	53.30	53.14	53.57	53.72
T	*Discoaster multiradiatus*	113.52	0.11	C24n.3n	0.540	53.30	53.14	53.57	53.72
	C24n.3n base	113.66	0.02	C24n.3n	0.570	53.32	53.16	53.58	53.74
	I1/I2 base	115.61			0.000	53.530	53.347	53.808	53.983
	H1-Elmo/H2 base	117.21	0.01	C24r	0.042	53.66	53.46	53.93	57.12
T	*Tribrachiatus contortus*	118.09	0.10	C24r	0.066	53.74	53.52	54.00	57.14
Tc	*Discoaster multiradiatus*	119.38	0.11	C24r	0.100	53.84	53.60	54.09	57.16
B	*Sphenolithus radians*	118.72	0.10	C24r	0.083	53.79	53.56	54.04	57.15
B	*Tribrachiatus orthostylus*	120.67	0.10	C24r	0.134	53.95	53.69	54.19	57.18
T	*Tribrachiatus bramlettei*	121.30	0.11	C24r	0.151	54.00	53.73	54.24	57.18
B	*Tribrachiatus contortus*	125.50	0.10	C24r	0.263	54.35	54.02	54.56	57.25
B	*Discoaster diastypus*	127.45	0.10	C24r	0.314	54.51	54.15	54.71	57.28
B	*Tribrachiatus bramlettei*	133.34	0.11	C24r	0.471	55.00	54.55	55.15	57.36
T	*Fasciculithus* spp./*F. tympaniformis*	135.87	0.11	C24r	0.538	55.21	54.72	55.35	57.40
T	*Rhomboaster* spp.	139.72	0.01	C24r	0.640	55.53	54.98	55.64	57.46

CPD
11, 4329–4389, 2015

Table 1. Continued.

Event		Site 1262 Depth (mcd)	Err (m)	AG07[e]/This study Chron	notation	W01 Age (Ma)	CK95 Age (Ma)	GTS04 Age (Ma)	GTS12 Age (Ma)
X	*Fasciculithus/Zygrhablithus*	139.80	0.02	C24r	0.643	55.54	54.99	55.64	57.46
Br	*Tribrachiatus bramlettei*	139.99	0.02	C24r	0.648	55.56	55.00	55.66	57.46
B	*Discoaster araneus*	–	–	–	–	–	–	–	–
B	*Rhomboaster* spp.	140.02	0.01	C24r	0.648	55.56	55.01	55.66	57.46
	PETM	140.13	0.02	C24r	0.652	55.57	55.01	55.67	57.46
	P/E boundary (extrapolated)	140.13	0.02	C24r	0.652	55.57	55.01	55.67	57.46
decrease	*Fasciculithus* spp.	140.13	0.02	C24r	0.652	55.57	55.01	55.67	57.46
T	*F. richardii* gr.	140.13	0.02	C24r	0.652	55.57	55.01	55.67	57.46
	? base	142.00	0.02	C24r	0.701	55.72	55.14	55.81	57.49
	D1/D2 base	146.17	0.02	C24r	0.812	56.07	55.42	56.13	57.55
	C1/C2 base	152.08	0.02	C24r	0.969	56.56	55.82	56.58	57.64
T	*Ericsonia robusta*	153.32	0.10	C25n	0.011	56.67	55.91	56.67	57.11
	C24r base	153.25			0.000	56.660	55.904	56.665	57.101
Bc	*F. alanii*	152.77	0.02	C24r	0.987	56.62	55.87	56.63	57.65
B	*Discoaster multiradiatus*	154.61	0.11	C25n	0.216	56.78	56.01	56.78	57.22
Tc	*Sphenolithus anarrhopus*	155.03	0.11	C25n	0.283	56.81	56.04	56.81	57.26
B	*Discoaster delicatus* gr.	156.92	0.11	C25n	0.583	56.97	56.19	56.97	57.42
	B1/B2 base	158.37	0.02	C25n	0.813	57.10	56.30	57.08	56.52
B	*Ericsonia robusta*	158.00	0.11	C25n	0.754	57.06	56.27	57.05	57.52
	C25n base	159.55			0.000	57.197	56.391	57.180	57.656
B	*Discoaster nobilis* gr.	157.35	0.10	C25n	0.651	57.01	56.22	57.00	57.46
B	*D. mohleri*	171.50	0.11	C25r	0.984	58.53	58.53	58.53	58.53
	C25r base	171.70			0.000	58.550	57.554	58.379	58.959

Reference calcareous nannofossil biozonations: [a]NP (Martini, 1971); [b] CP (Okada and Bukry, 1980); [c] CN (Agnini et al., 2014).
Reference timescales: W01 (Westerhold et al., 2008 – option1); CK95 (Cande and Kent, 1995); GTS04 (Ogg and Smith, 2004); GTS12 (Ogg, 2012).
[d] DARM09 (Dallanave et al., 2009).
[e] AG07 (Agnini et al., 2007)

CPD
11, 4329–4389, 2015

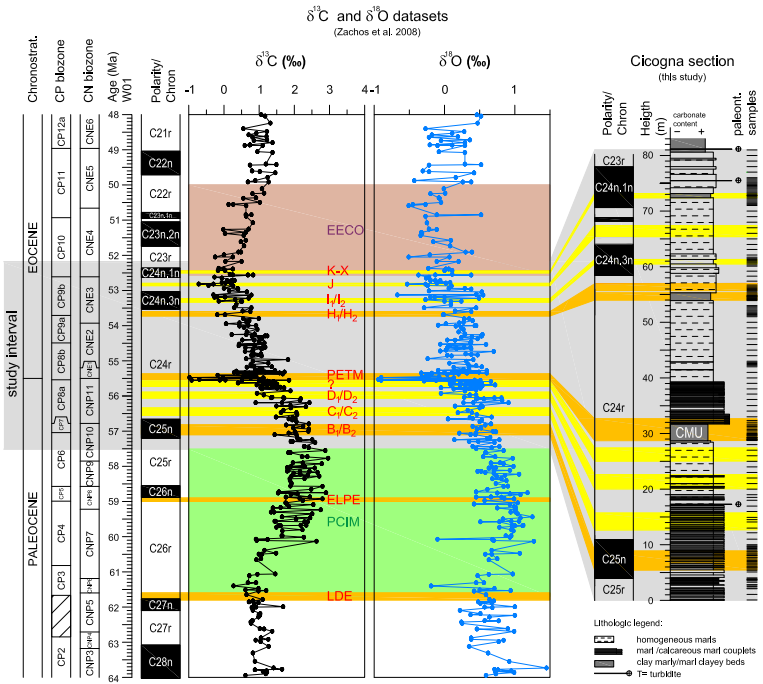

Figure 1. Middle Paleocene to middle Eocene (64 to 48 Ma) stable isotope ($\delta^{13}C$ and $\delta^{18}O$) records of benthic foraminifera from multiple locations (Zachos et al., 2008) placed on the Option 1 (W01) time scale of Westerhold et al. (2008). Also shown are positions of polarity chrons and calcareous nannofossil biozones for this time interval, both from the CP Biozone scheme (Okada and Bukry, 1980) and the CN Biozone scheme (Agnini et al., 2014). Various "events" are noted within this chronostratigraphic framework, including the Paleocene carbon isotope maximum (PCIM), the Paleocene-Eocene thermal maximum (PETM), the H-1/ETM-2 event, the K/X event, and the Early Eocene climatic optimum (EECO). To the right is the general lithologic column and magnetostratigraphy of the Cicogna section (Dallanave et al., 2009).

CPD
11, 4329–4389, 2015

Stable isotope and calcareous nannofossil assemblage records

C. Agnini et al.

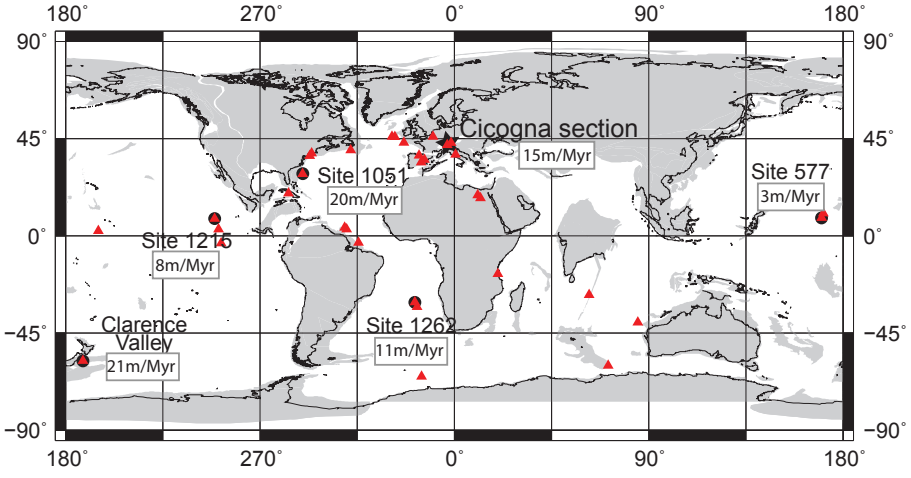

55 Ma Reconstruction

CPD
11, 4329–4389, 2015

Figure 2. Paleogeographic map indicating approximate locations at 55 Ma for several key sites with detailed stable isotope records across the late Paleocene and early Eocene. These include (marked with black dots and star) the Cicogna section (NE Italy, this study), DSDP Site 577 (Shastky Rise, Dickens and Backman, 2013;), ODP Sites 1051 (Blake Nose, Ogg and Bardot, 2001), 1215 (central Pacific, Raffi et al., 2005), and 1262 (Walvis Ridge, Westerhold et al., 2008), and the Clarence Valley (CV) sections New Zealand, (Dallanave et al., 2015). The grey areas represent plate fragments, while the black lines show present-day shorelines. Boxes next to site locations show average compacted sedimentation rates from the base of Chron C25n to the base of Chron C23r (57.20–52.36 Ma). The base map comes from the ODSN web site (http://www.odsn.de/odsn/services/paleomap/paleomap.html). Red triangles are locations where a decrease in diversity of *Fasciculithus* spp. has been documented near the PETM. The particular locations are the Clarence Valley sections, central Pacific (ODP Site 1215, 1220, 1221), western Pacific (Shatsky Rise, DSDP Site 577 and ODP Site 865), South Atlantic (Walvis Ridge, DSDP Site 527, ODP Sites 1262, 1263–1267; Maud Rise, ODP Site 690), equatorial Atlantic (Ceara Rise, ODP Site 929; Demerara Rise, ODP Sites 1259, 1260), northwestern Atlantic (New Jersey Margin land sections, ODP Site 1051; IODP Site U1403, U1409), northeastern Atlantic (Bay of Biscay DSDP Sites 401 and 549, 550, Zumaya land section), Indian Ocean (DSDP Site 213; ODP 672; Kerguelen Plateau, ODP Site 1135) (Backman, 1986; Aubry, 1999; Bralower, 2002; Dupuis et al., 2003; Tremolada and Bralower, 2004; Bralower and Mutterlose, 1995; Monechi et al., 2000; Gibbs et al., 2004; Raffi et al., 2005; Agnini et al., 2007a; Angori et al., 2007; Mutterlose et al., 2007; Jiang and Wise, 2009; Shamrock, 2010; Norris et al., 2014; Dallanave et al., 2015).

CPD
11, 4329–4389, 2015

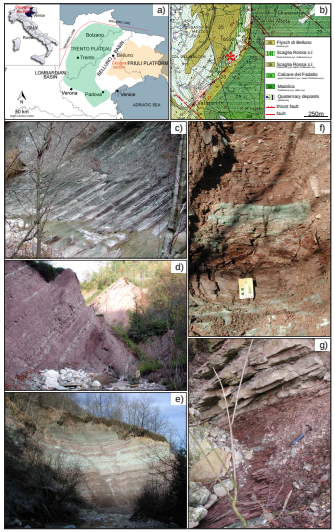

Figure 3. The location and representative photographs of the Cicogna section in northeast Italy. **(a)** Geographic map showing the main late Cretaceous–early Paleogene paleogeographic domains of the Italian Southern Alps (modified after Cati et al., 1989); **(b)** geological map of the local area (modified after Costa et al., 1996 indicating also the location of the Cicogna section (red asterisk); **(c)** alternating beds of Paleocene gray-green marls and calcareous marls (0–20 m); **(d)** marl/calcareous marl couplets in the lower Eocene portion of the section (approximately 40.0–70.0 m); **(e)** the Scaglia Rossa *sensu latu* overlain by the Belluno Flysch; **(f)** the base of the Clay Marl Unit, which denotes the onset of the PETM (approximately 28.7–29.3 m); **(g)** the brownish-red interval of clayey marls with sporadic grey-green cm-scale spots and lenses, the CMU, overlaid by prominent rhythmic alternations of marls and calcareous marls (approximately 28.7–33.0 m).

CPD
11, 4329–4389, 2015

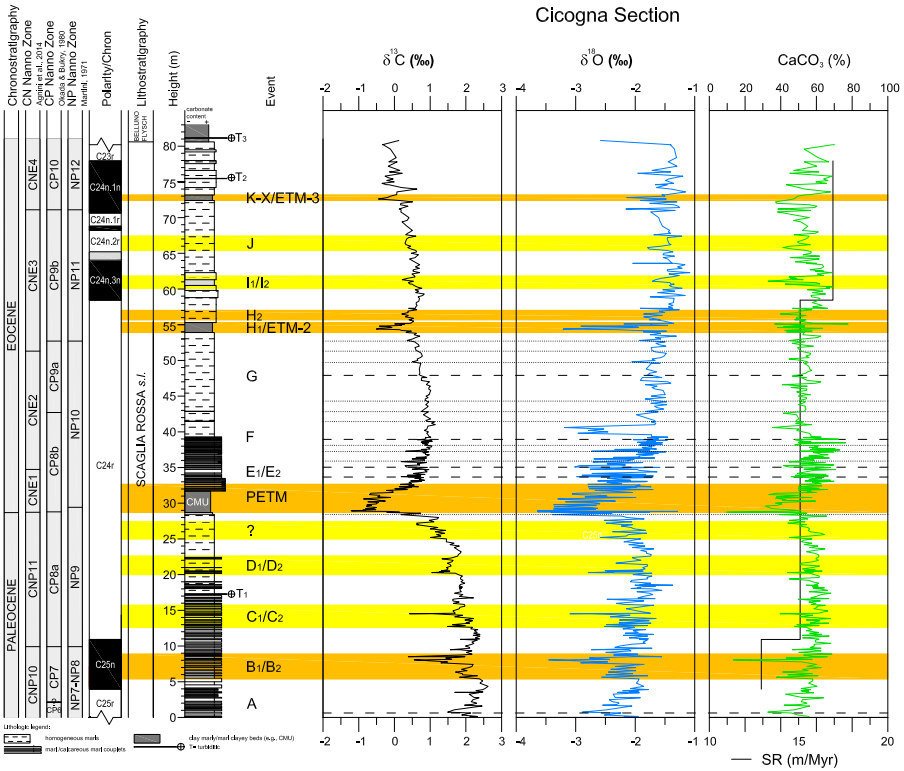

Figure 4. The Cicogna section with records of bulk carbonate $\delta^{13}C$ and $\delta^{18}O$ data, and $CaCO_3$ content. {*Calcareous nannofossil biostratigraphy (CP and NP biozones) and magnetostratigraphy are after Dallanave et al. (2009), CN biozones are also reported. Orange and yellow bands mark major $\delta^{13}C$ excursions.*} Dashed lines highlight minor $\delta^{13}C$ events that have been labeled elsewhere (e.g., E1/E2, F and G; Cramer et al., 2003), whereas dotted lines indicate minor changes $\delta^{13}C$ profile excursions that appear to occur at ODP Site 1262 (see also Fig. 5).

CPD
11, 4329–4389, 2015

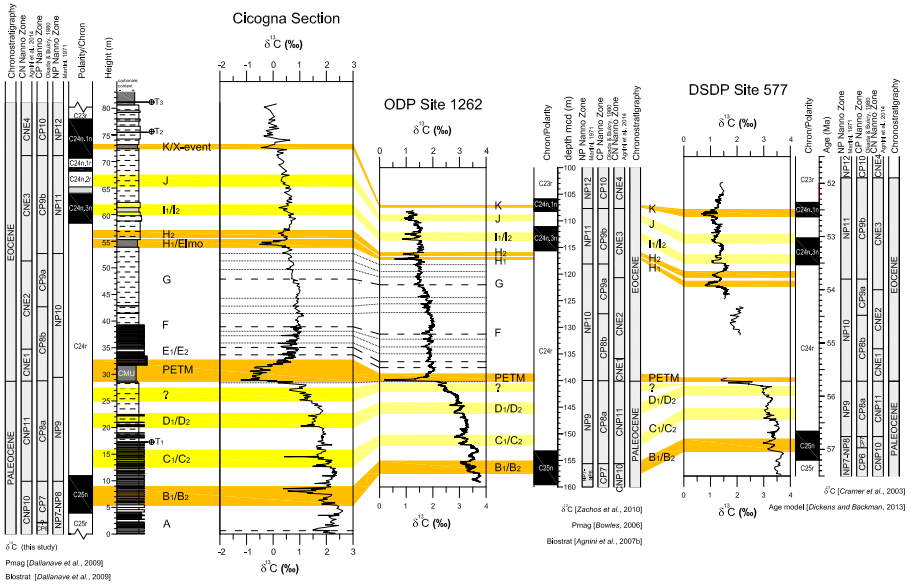

Figure 5. Stratigraphic correlation between upper Paleocene and Lower sections at Cicogna, ODP Site 1262 (Zachos et al., 2010), and DSDP Site 577 (Cramer et al., 2003; Dickens and Backman, 2013). All three sites have independently derived nannofossil datums, polarity chrons and $\delta^{13}C$ records, which account for subtle temporal offsets.

CPD
11, 4329–4389, 2015

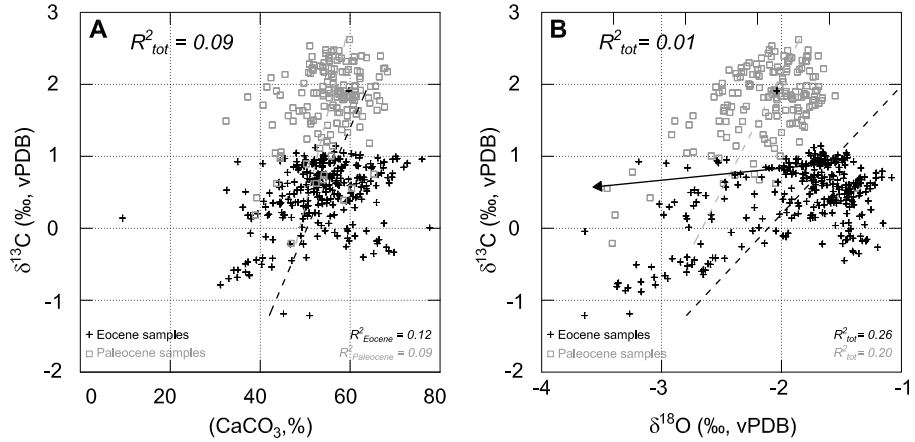

Figure 6. Plots of **(a)** δ^{18}O vs. δ^{13}C, and **(b)** $CaCO_3$ vs. δ^{13}C for samples from the Cicogna section. The black arrow shows the effect of burial diagenesis.

CPD
11, 4329–4389, 2015

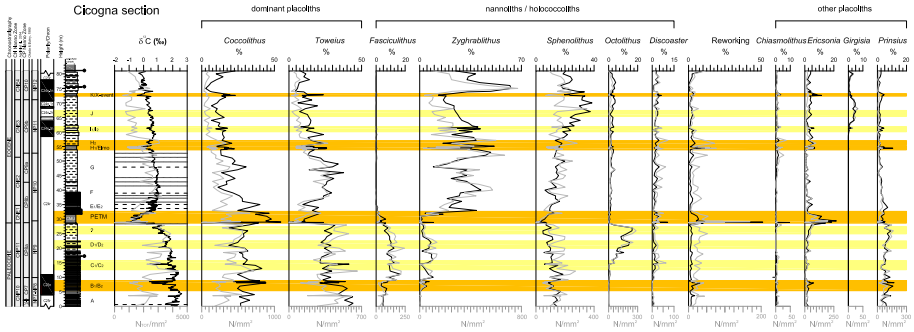

Figure 7. Relative (%) and semi-quantitative ($N\,mm^{-2}$) abundances of selected calcareous nannofossil genera are plotted against lithostratigraphy, magnetostratigraphy, biostratigraphy and carbon isotope ($\delta^{13}C$) stratigraphy at the Cicogna section. Orange and yellow bands mark CIEs shown in previous figures.

CPD
11, 4329–4389, 2015

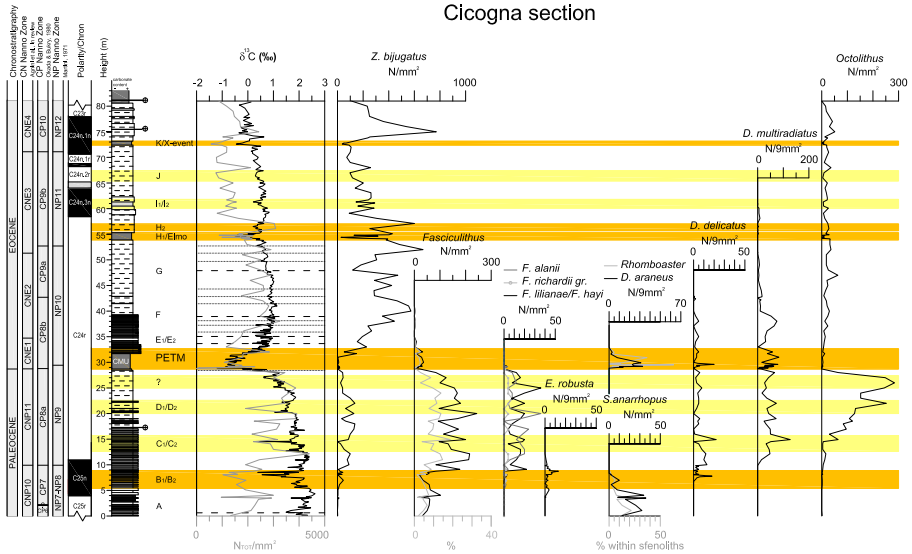

Figure 8. Relative (%) and semi-quantitative ($N\,mm^{-2}$) abundances of selected, mainly late Paleocene, calcareous nannofossil taxa plotted against lithostratigraphy, magnetostratigraphy, biostratigraphy and carbon isotope ($\delta^{13}C$) stratigraphy at the Cicogna section. Orange and yellow bands mark CIEs shown in previous figures.

CPD
11, 4329–4389, 2015

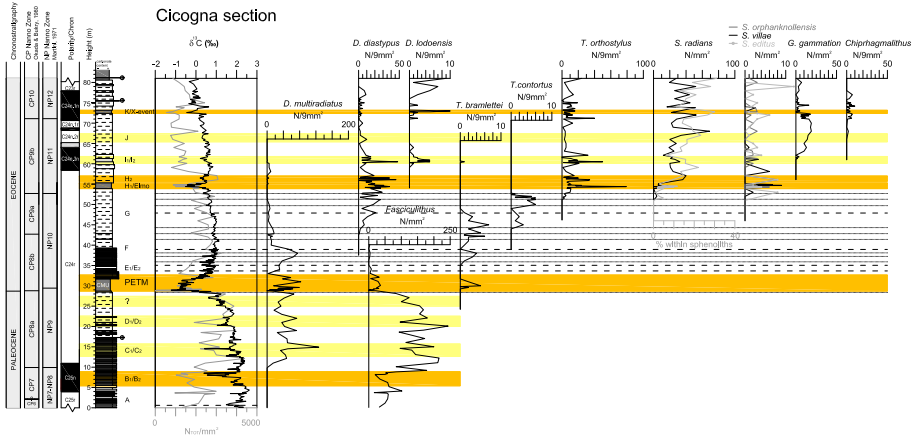

Figure 9. Relative (%) and semi-quantitative (N mm^{-2}) abundances of selected, mainly early Eocene, calcareous nannofossil taxa are plotted against lithostratigraphy, magnetostratigraphy, biostratigraphy and carbon isotope (δ^{13}C) stratigraphy at the Cicogna section together. Orange and yellow bands mark CIEs shown in previous figures.

CPD
11, 4329–4389, 2015

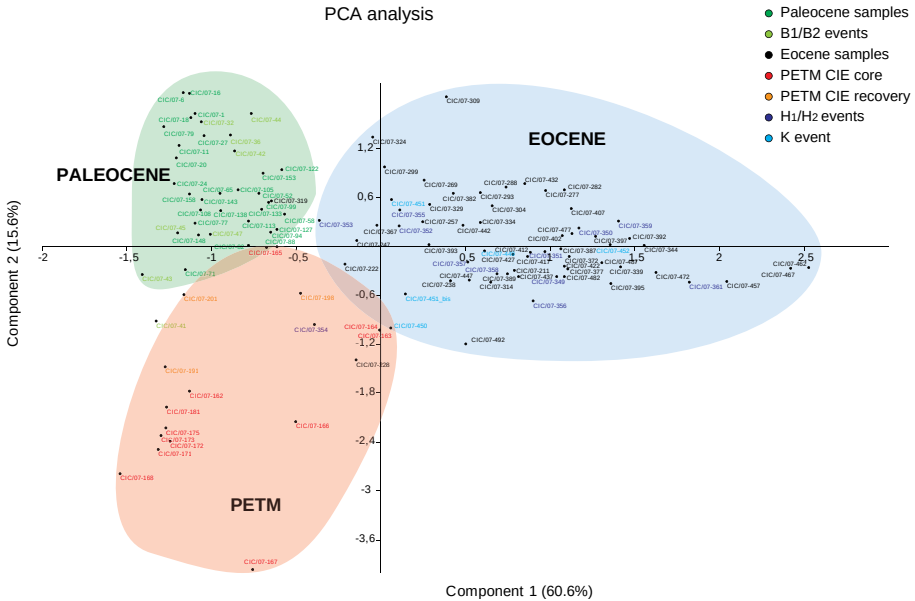

Figure 10. Principal Component Analysis (PCA) of calcareous nannofossil percentage data of the Cicogna section. Calcareous nannofossils are subdivided into 15 subgroups (*Chiasmolithus, Coccolithus, Ellipsolithus, Discoaster, Ericsonia, Fascicuithus, Girgisia, Octolithus, Prinsius, Sphenolithus, Toweius, Rhomboaster/Tribrachiatus, Zyghrablithus*, reworking, others). Scatter plot of percentage data of calcareous nannofossil taxa of samples from the Cicogna section in terms of the first and second component. Each sample is represented by a circle and labelled. Different colors serve to separate sub-sets of samples having the same age.

CPD
11, 4329–4389, 2015

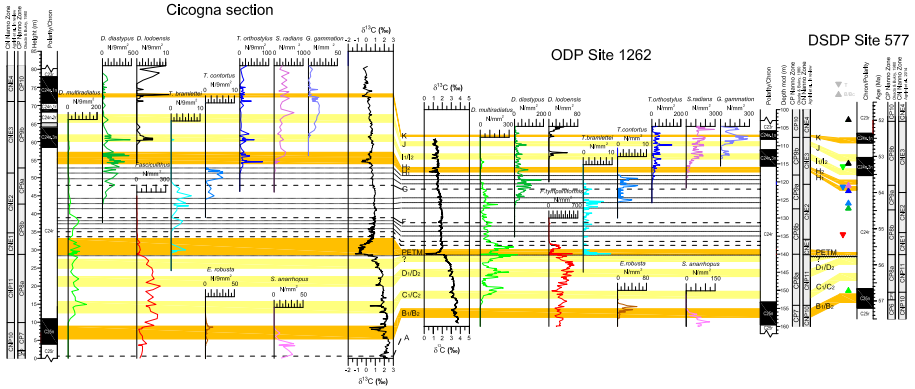

Figure 11. Comparison of $\delta^{13}C$ profiles and semi-quantitative abundance patterns of selected calcareous nannofossil taxa from the Cicogna section and ODP Site 1262. Calcareous nannofossil biohorizons from DSDP Site 577 are reported in the right part of the figure. Orange and yellow bands mark CIEs shown in previous figures.

CPD
11, 4329–4389, 2015

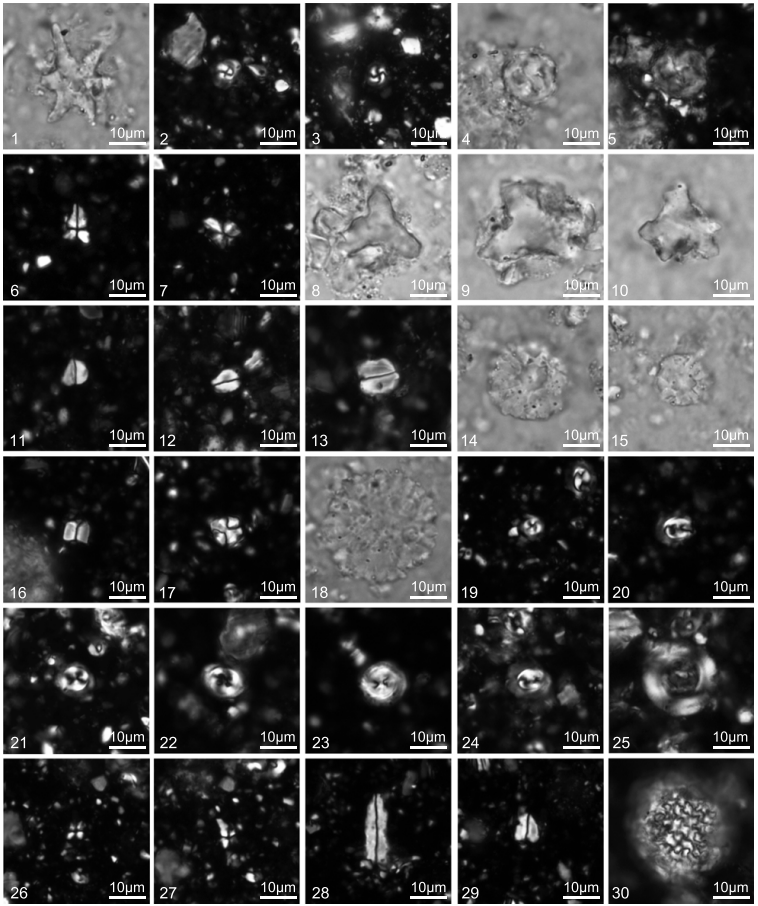

CPD
11, 4329–4389, 2015

Plate 1. Images of selected calcareous nannofossil taxa from samples of the Cicogna section. Scale bar 10 µm. **1.** *Discoaster lodoensis* Bramlette and Riedel, 1954. Parallel light. Sample CIC/07-492. **2–3.** *Girgisia gammation* (Bramlette Sullivan, 1961) Varol, 1989. Crossed nicols. Sample CIC/07-437. **4–5.** *Chiphragmalithus calathus* Bramlette and Sullivan, 1961; 4. Parallel light; 5. Crossed nicols. Sample CIC/07-447. **6–7.** *Sphenolithus radians* Deflandre in Grassé, 1952. 6. Crossed nicols 0°; 7. Crossed nicols 45°. Sample CIC/07-437. **8.** *Tribrachiatus orthostylus* Shamrai, 1963. Parallel light. Sample 208-1262A-11H- 1, 149. Sample CIC/07-447. **9–10.** *Tribrachiatus contortus* (Stradner, 1958) Bukry, 1972. Parallel light. Sample CIC/07-335. **11–13.** *Zyghrablithus bijugatus* (Deflandre in Deflandre and Fert, 1954) Deflandre, 1959. Crossed nicols. Sample CIC/07-437. **14.** *Discoaster salisburgensis* Stradner, 1961. Parallel light. Sample CIC/07-335. **15.** *Discoaster diastypus* Bramlette and Sullivan, 1961. Parallel light. Sample CIC/07-335. **16.** *Fasciculithus tympaniformis* Hay and Mohler in Hay et al., 1967. Crossed nicols. Sample CIC/07-335. **17.** *Octolithus multiplus* (Perch-Nielsen, 1973) Romein, 1979. Crossed nicols. Sample CIC/07-122. **18.** *Discoaster multiradiatus* Bramlette and Riedel, 1954. Parallel light. Sample CIC/07-122. **19.** *Toweius pertusus* (Sullivan, 1965) Romein, 1979. Crossed nicols. Sample CIC/07-122. **20.** *Toweius occultatus* (Locker, 1967) Perch-Nielsen, 1971. Crossed nicols. Sample CIC/07-122. **21.** *Toweius eminens* (Bramlette and Sullivan, 1961) Perch-Nielsen, 1971. Crossed nicols. Sample CIC/07-029. **22.** *Toweius eminens* (Bramlette and Sullivan, 1961) Perch-Nielsen, 1971. Crossed nicols. Sample CIC/07-029. **23.** *Toweius eminens* (Bramlette and Sullivan, 1961) Perch-Nielsen, 1971. Crossed nicols. Sample CIC/07-122. **24.** *Prinsius bisulcus* (Stradner, 1963) Hay and Mohler, 1967. Crossed nicols. Sample CIC/07-029. **25.** *Ericsonia robusta* Bramlette and Sullivan, 1961. Crossed nicols. Sample CIC/07-029. **26-27.** *Sphenolithus anarrhopus* Bukry and Bramlette, 1969. 24. Crossed nicols 0°; 25. Crossed nicols 45°. Sample CIC/07-029. **28–29.** *Zyghrablithus bijugatus* (Deflandre in Deflandre and Fert, 1954) Deflandre, 1959. Crossed nicols. Sample CIC/07-122. **30.** *Thoracosphaera saxea* (Stradner, 1961). Crossed nicols. Sample CIC/07-122.

CPD
11, 4329–4389, 2015